Title: Hematopoietic stem and progenitor cells improve survival from sepsis by boosting immunomodulatory cells.

Authors: Daniel E. Morales-Mantilla[1,2], Bailee Kain[2,3], Duy Le[1,2], Anthony R. Flores[4], Silke Paust[5], Katherine Y. King[1,2,3]

[1]Graduate Program in Immunology, Baylor College of Medicine, Houston, TX

[2]Department of Pediatrics, Division of Infectious Diseases, Baylor College of Medicine, Houston, TX

[3]Graduate Program in Translational Biology and Molecular Medicine, Baylor College of Medicine, Houston TX

[4]Division of Infectious Diseases, Department of Pediatrics, UTHSC/McGovern Medical School, Houston, TX

[5]The Scripps Research Institute, Department of Immunology and Microbiology, La Jolla, CA

Corresponding author

Katherine Y. King, MD, PhD

1102 Bates Ave.

Feigin Tower Suite 1150

Houston, TX, 77030

United States

(832) 824-4330

kyk@bcm.edu

Abstract

New therapeutic strategies to reduce sepsis-related mortality are urgently needed, as sepsis accounts for 1 in 5 deaths worldwide. Since hematopoietic stem and progenitor cells (HSPCs) are responsible for producing blood and immune cells, including in response to immunological stress, we explored their potential for treating sepsis. In a mouse model of Group A *Streptococcus* (GAS)-induced sepsis, severe immunological stress was associated with significant depletion of bone marrow HSPCs and mortality within approximately 5-7 days. We hypothesized that the inflammatory environment of GAS infection drives rapid HSPC differentiation and depletion that can be rescued by infusion of donor HSPCs. Indeed, infusion of 10,000 naïve HSPCs into GAS-infected mice resulted in rapid myelopoiesis and a 50-60% increase in overall survival. Surprisingly, mice receiving donor HSPCs displayed a similar pathogen load compared to untreated mice. Flow cytometric analysis revealed a significantly increased number of myeloid-derived suppressor cells in HSPC-infused mice, which correlated with reduced inflammatory cytokine levels and restored HSPC levels. These findings suggest that HSPCs play an essential immunomodulatory role that may translate into new therapeutic strategies for sepsis.

Introduction

Sepsis accounts for one in five deaths worldwide and is a common final pathway for many disease processes such as cancer, diabetes, and cardiovascular disease (1). Sepsis is an inflammatory syndrome largely driven by the activation of immune cells by pathogen associated molecular patterns (PAMPs) and damage-associated molecular patterns (DAMPs) (2,3). After recognizing these molecules via pattern recognition receptors (PRR), immune cells become activated and produce proinflammatory cytokines, notably interleukins IL-1, IL-6, interferons (IFNs), and tumor necrosis factor that contribute to fever, vasodilation, and multiorgan dysfunction (3–6). For patients that progress to septic shock, mortality rates remain as high as 40% (7).

Leukopenia is a feature of severe sepsis that arises from apoptosis of peripheral immune cells and is an independent risk factor for death. To counteract the adverse effects of leukopenia, investigators have used immunotherapies such as GM-CSF (8) or granulocyte infusions in an attempt to restore leukocyte numbers and improve survival. These strategies have produced mixed results (9–11). The benefits of granulocyte infusions in cancer patients with fever and neutropenia are limited by the difficulty of obtaining sufficient cells and the short-lived nature of those cells (12,13).

Recent work from our group and others indicates that hematopoietic stem and progenitor cells (HSPCs) express surface receptors for cytokines, chemokines, and pathogen-associated molecular patterns (PAMPs) (14–21) and respond rapidly upon direct and indirect stimulation by these signals. HSPCs, the progenitors of all blood and immune cells, are comprised of five subgroups of hematopoietic cells: hematopoietic stem cells (HSC) which have long term self-renewal capacity, and four types of multipotent progenitors (MPP 1-4), which are defined by lower self-renewal capacity and myeloid or lymphoid differentiation biases (6,22–26). Immune responses induce HSPCs in the bone marrow (BM) to produce effector immune cells via a process

called emergency hematopoiesis (18,20–22,27,28). The capacity of HSPCs to directly detect pathogen-derived molecules, cytokines, and chemokines suggests that emergency granulopoiesis can be mobilized from even the most primitive hematopoietic progenitors and that HSPCs have an active role in fighting infections. However, the extent and mechanism by which HSPC responses contribute to immunity in the acute setting remain poorly defined.

We recently showed that chronic inflammatory stress impairs HSPC quiescence and self-renewal while promoting their activation and terminal differentiation (28). Upon direct sensing of inflammatory cytokines such as interferon gamma (IFNγ), HSCs are dislodged from their normal position near quiescence-enforcing CXCL12-abundant reticular cells in the niche. Inflammatory signaling induces transcription factors such as Pu.1, CEBPb, and BATF2 (18,20,28,29) to promote myeloid differentiation, leading to the expansion of granulocyte and monocyte populations. Disruption of the homeostatic balance of self-renewal and differentiation eventually leads to depletion of the progenitor compartment (20,22,28). Collectively, these studies point toward a direct role for HSPCs in supplying the myeloid cells critical to the immune response against infection.

To test their contribution to immune responses during acute infection, we examined the role of HSPCs in a mouse model of *Streptococcus pyogenes* infection, also known as Group A *Streptococcus* (GAS). GAS is a common pathogen that causes a plethora of diseases, from mild skin infections to life-threatening necrotizing fasciitis and sepsis (6,30–32). GAS infections can infiltrate the bloodstream and other organs, causing high systemic levels of inflammatory cytokines including IFNγ, TNF, IL-1, and IL-6. As HSPCs have been shown to activate and differentiate in response to these cytokines (15,18,20–22,33–35), in this study we sought to determine the role of HSPCs in immune responses against infections.

Here we found that GAS infection significantly depletes HSPCs in the bone marrow. We tested the idea of infusing HSPCs to restore the hematopoietic progenitor pool. Mice treated with

HSPCs showed restored HSPC numbers in the BM, increased myeloid cell production, and significantly improved overall survival. Surprisingly, HSPC infusion did not reduce pathogen burden. Instead, HSPC infusion correlated with a significant increase in the abundance of myeloid-derived suppressor cells (MDSCs) and a dampening of overall systemic inflammation. In summary, our studies indicate that HSPCs contribute to survival from sepsis by supporting the production of immunosuppressive MDSCs.

Results

GAS infection induces trafficking of myeloid cells from the BM into circulation.

To characterize the impact of acute infections on the hematopoietic system, we inoculated mice by intramuscular injection of the hind leg with $2x10^6$ colony forming units (CFU) of the model pathogen *S. pyogenes* strain MGAS315. To characterize differentiated hematopoietic populations during infection, we performed flow cytometric analysis of BM and peripheral blood (PB) lineage cells 24h after GAS infection (**Figure 1A**) and collected serum for cytokine analyses. BM characterization of lineage cells showed a significant decrease in BM monocytes (**Figure 1C**) and granulocytes (**Figure 1D**) with no change in BM B- or T cells (**Figure 1E & 1F**). In contrast, PB lineage composition was significantly skewed towards myeloid cells with significantly higher circulating monocytes and granulocytes (**Figure 1G & 1H**) and lower lymphoid cells (**Figure 1I & 1J**). Serum cytokine characterization showed a significant increase in monocyte chemoattractant protein-1 (MCP-1; also known as CCL2) (**Figure 1B**). These results suggest that myeloid cells exit the BM into circulation following an MCP-1 gradient, consistent with prior studies showing MCP-1-driven mobilization during inflammation (36,37).

GAS infection depletes bone marrow HSPCs without evidence of extramedullary hematopoiesis.

After 24h of infection, the state of HSPCs in the infected mice were analyzed by flow cytometry of bone marrow (BM) and spleen (**Figure 2A**) (See **Table 1** for surface markers). BM cells were not gated for the common stem cell marker SCA1 (**Figure 2B**), since it has been previously described to be non-specifically expressed during inflammatory stress (19). The total number of HSPCs dropped significantly in just 24 hours in GAS-infected mice (**Figure 2C**). More specifically, HSPC subpopulations including HSCs, multipotent progenitor 3 (MPP3s), and MPP4s were significantly lower in GAS-infected mice (**Figure 2D, 2E, and 2F**).

Extramedullary hematopoiesis is the proliferation and differentiation of HSCs in tissues other than the bone marrow, the canonical stem cell niche. The spleen is one of the most common sites of extramedullary hematopoiesis during infections (38). To assess whether a reciprocal increase in extramedullary hematopoiesis accompanied loss of HSPCs in the BM, we analyzed spleen tissue by flow cytometry. While there was a slight increase in total HSPCs in the spleen (**Figure 2G**), there was no significant change in spleen populations that include HSCs/MPP1, MPP2s, or MPP3/4 (**Figure 2H-2J**). This finding suggests that the loss of BM HSPC populations is not simply a result of migration from the BM into the spleen.

GAS infection induces HSC myeloid differentiation.

Activation of HSPCs by PAMPs or cytokines promotes their proliferation and differentiation (16,18,20–22,39). To determine the lineage fate of endogenous HSPCs following GAS infection, we performed lineage tracing experiments using the tamoxifen-inducible KRT18-CreERT2 : Rosa26-lox-STOP-lox-TdTomato mouse system (**Figure 3A**). Within the BM, *Krt18* is almost exclusively expressed in HSCs (40) and these mice do not have any immunological impairment that would change the severity of our infection model. Tamoxifen induction activates the CreERT2 protein in Krt18-expressing HSCs, resulting in irreversible TdTomato expression in HSCs and their newly formed progeny (**Figure 3B**).

After five days of intraperitoneal injections of tamoxifen, mice were inoculated with GAS or saline. Since the average mammalian cell cycle takes 24h, we decided to trace the lineage of hematopoiesis 72h post GAS infection. After these 72 hours, BM and PB was harvested for flow cytometric analysis. Analysis of the BM showed that GAS infection induced the production of new HSPCs, which includes short term HSCs and MPPs (**Figure 3C-3D**). In addition, there was significant labeling of CD41+ HSCs, a myeloid-biased and proinflammatory subset of HSCs (**Figure 3E**) (41) and new cells of the myeloid lineage (**Figure 3F-3H).** While we found a significant

increase in new BM monocytes (**Figure 3G**), there was no significant change in the frequency of TdTomato-labeled granulocyte/monocyte progenitors (GMPs) (**Figure 3I**), which may simply reflect a rapid flow through this compartment to terminally differentiated populations. We also saw no statistically significant increase in BM granulocytes (**Figure 3H**); however, PB analysis showed a significant increase in new myeloid cells in both monocytic and granulocytic branches (**Figure 3L-3N**). While there was a significant decrease in the production of new BM T cells (**Figure 3J**), there was no change in BM B cells (**Figure 3K**) nor PB T or B cells (**Figure 3O-P**). These data suggest that endogenous HSCs undergo rapid emergency myelopoiesis during GAS infection.

HSPC infusion promotes survival in GAS-infected mice.

Given that HSPCs are activated to divide and differentiate into immune effector cells upon inflammatory stimulation and we observed an acute loss of HSPCs in GAS-infected mice, we hypothesized that infusion of naïve HSPCs (Lin- Sca-1+ c-Kit+) into GAS-infected mice could improve pathogen clearance, reduce tissue damage, and prolong survival. To test this hypothesis, we infected mice with $2x10^6$ CFU MGAS315 and then infused 10,000 FACS-purified HSPCs 24h later, when endogenous HSPCs are significantly decreased (**Figure 4A**). This HSPC dose, equivalent to approximately $1.7x10^7$ cells per m^2 body surface area, is significantly lower than the dose used for granulocyte infusions, typically between 10^8-10^{10} cells per m^2 (42). On day three post-infection, we harvested BM, limb tissue, and spleen to characterize BM populations and pathogen load (**Figure 4B**).

BM characterization showed that HSPC infusion restored the relative abundance of HSPCs, HSCs, and myeloid-biased progenitors, such as MPP3s and GMPs, in the BM (**Figure 4C-4H**. We observed that GAS-infected mice that received HSPCs showed lower morbidity than non-rescued mice, with improved overall body score and activity level. To assess survival, we performed Kaplan-Meier survival studies of GAS-infected mice in the absence or presence of

HSPC rescue (**Figure 4K**). GAS infected mice infused with HSPCs had significantly higher survival than non-rescued mice (**Figure 4L**). However, to our surprise, HSPC infusion did not significantly affect the pathogen burden in the infected muscle (**Figure 4I**) or pathogen spread to other tissues (**Figure J**). Overall, these findings suggest that HSPC infusion is beneficial during GAS infections and promotes survival by a mechanism other than pathogen clearance.

Superinfection further depletes HSPCs in mice.

To determine the extent of the protective potential of HSPC infusion during infections, we tested the efficacy of HSPC rescue in a mouse model of influenza and GAS superinfection. Here we used a model of influenza and *Streptococcus pyogenes* (strain MGAS315) bacterial superinfection. Mice were infected with influenza (strain H1N1 PR8) by intranasal injection of 150 plaque-forming units (PFU). On day three post influenza virus infection, which represents peak viral replication for humans and mice (43,44), we injected mice with $2x10^6$ CFU MGAS315 by IM inoculation (**Supplemental figure 1A**). On day four (24h post GAS infection), we analyzed bone marrow and PB. Lin- cells in the BM showed phenotypical differences in surface expression of Sca-1 and c-Kit proteins depending on the pathogen combination (19) (**Supplemental figure 1B**). In addition, superinfection caused a severe decrease in HSPCs and their subpopulations (**Supplemental figure 1C-1H**). Most notably, the absolute number of HSCs was reduced to 20-30% of a healthy mouse (**Supplemental figure 1D**).

We also analyzed BM and PB lineage populations of superinfected mice (**Supplemental figure 2A**). Similar to GAS-infected mice, superinfection led to an increase in serum levels of MCP-1 (**Supplemental figure 2B**) that resulted in the exit of BM monocytes and BM granulocytes (**Supplemental figure 2C & 2G**) into circulation (**Supplemental figure 2D & 2H**). BM B cell and T cell numbers did not change (**Supplemental figure 2E & 2I**), while the abundance of circulating

B and T cells was reduced in GAS infected and superinfected mice (**Supplemental figure 2F & 2J**).

HSPC infusion promotes survival in superinfected mice and increases levels of HSPCs and myeloid progenitors in the BM.

The loss of HSPCs and HSCs was very prominent in superinfected mice, more so than in mice infected with GAS alone. Therefore, we hypothesized that an infusion of 10,000 HSPCs would also benefit mice in this model of superinfection (**Figure 5A**). As expected, HSPC infusion significantly increased HSPCs and myeloid-biased progenitors in superinfected mice (**Figure 5B-5G**). As seen in GAS-infected mice, HSPC infusion did not promote bacterial (**Figure 5H**) or viral (**Figure 5I**) clearance in superinfected mice. The spread of bacteria to the spleen was also unaffected by HSPC infusion (**Figure 5J**).

Despite the severity of the infection, superinfected mice that received an HSPC infusion (**Figure 5K**) had significantly improved survival compared to non-rescued mice (**Figure 5L**). This finding suggests that the protective properties of HSPC infusion are effective even in this very severe model of infection.

HSPC infusion increases immunomodulatory MDSCs and prevents sepsis-induced cytokine exacerbation.

Production of proinflammatory cues including IL1, IL6, IL8, TNF, and MIP1a is a key driver of morbidity during sepsis. Together, these cues contribute to systemic inflammatory response syndrome (SIRS), including fever, tachypnea, vasodilation, and circulatory collapse (5,45). These cytokines are independently associated with poor outcomes and death from sepsis in humans. Since we observed improved survival in mice receiving HSPC infusion without any changes in

pathogen load, we hypothesized that HSPCs could impact immunomodulatory cell composition and the inflammatory response to severe infection. Upon analysis of PB and BM populations after HSPC infusion (**Figure 6A**), there were no changes in BM or PB T lymphocytes that could indicate a Treg-related activity (**Supplemental Figure 3A & 3B**). However, we found that HSPC infusion significantly increased PB PMN-MDSCs (**Figure 6B**) and restored PB M-MDSCs levels (**Figure 6C**). Similarly, HSPC infusion restored BM PMN-MDSCs and M-MDSCs populations in GAS-infected mice (**Figure 6D & 6E**). These cells were functionally validated (**Supplemental figure 3C**) as immunosuppressive cells by their ability to reduce activated T cell proliferation in culture (**Supplemental figure 3D**). Strikingly, cytokine profiling 72 hours after GAS infection showed reduced overall levels of proinflammatory cytokines in GAS-infected mice that received HSPC infusion (**Figure 6F**). These findings suggest that HSPC infusion supports the production of MDSC populations sufficient to dampen maladaptive proinflammatory cues during sepsis.

Infused HSPCs do not engraft but produce myeloid cells including MDSCs.

In order to determine whether infused HSPCs directly differentiate into MDSCs, we performed lineage tracing experiments using expression of the CD45.1 variant to distinguish infused HSPCs from endogenous cells. Thirty days after infusion, the CD45.1+ cell compartment showed no HSCs but a low number of MPP1 and myeloid biased MPP3s in the BM (**Figure 7A**). Lineage analysis in the BM showed that these cells gave rise to more myeloid cells compared to lymphoid. Furthermore, a fraction of the cells became new monocytic-MDSCs (M-MDSCs) and polymorphonuclear-MDSCs (PMN-MDSCs) (**Figure 7B**). Upon examination of the peripheral blood, circulating CD45.1 were primarily myeloid cells, with a small fraction identified as M-MDSCs and PMN-MDSCs (**Figure 7C**). Collectively, these data show that infused cells differentiate towards the myeloid lineage with no sign of stem cell engraftment. Whereas MDSCs did arise directly from infused cells, their numbers were not sufficient to account for the large

increase in MDSCs observed in the HSPC-rescued mice. These data suggest that HSPC infusion contributes to MDSC expansion via both direct and indirect mechanisms.

Discussion

Here, we show HSPC infusion holds therapeutic potential for bacterial sepsis. Our studies demonstrate that GAS infection induces a robust myeloid response just 24 hours after infection and significantly depletes HSPC populations in the bone marrow. After infection, endogenous HSPCs are driven to differentiate towards the myeloid lineage. However, this response is insufficient to prevent disease progression and pathogen dissemination, resulting in mortality in 5-7 days. While sepsis has been described to cause mobilization of HSPCs (46), we did not find any evidence of HSC or MPP mobilization to the spleen. Strikingly, we found infusing just 10,000 HSPCs improved survival in GAS-infected mice and mice with GAS and influenza superinfection. This infusion was capable of increasing PB and BM hematopoietic populations of infected mice. Specifically, HSPC infusion restored BM HSPCs and both PB and BM MDSC populations. Importantly, HSPC infusion did not reduce pathogen burden, but contributed to survival via the generation of immunoregulatory cells that dampened maladaptive inflammatory signaling in infected mice.

The hematopoietic and immune systems are comprised of immune cells with antimicrobial killing capacity as well as various types of immunomodulatory cells such as MDSCs, regulatory B cells (Bregs), and regulatory T cells (Tregs) (47–49). In the short time-frame of acute sepsis, myeloid cells such as neutrophils, monocytes, and macrophages are of critical importance in rapidly recognizing and killing invading bacteria. Our data demonstrate that these cells and even the progenitors that produce them in the bone marrow can be rapidly depleted during a severe acute infection. Furthermore, lineage tracing experiments provide the first direct evidence that terminally differentiated myeloid cells are rapidly produced from the level of the HSC during an acute infection. Initially we hypothesized that replacement of HSPCs may improve outcomes from acute bacterial infection by boosting the availability of myeloid cells to kill bacteria. While myeloid

cell populations were somewhat restored after HSPC infusion, this was insufficient to reduce pathogen burden.

Dysregulated inflammation is one of the main drivers of morbidity and mortality during infections (5,50–52). For example, excessive inflammatory responses are a common result of seasonal influenza (4,50) and SARS-CoV-2 infection (51). Seasonal influenza increases the susceptibility of patients to secondary bacterial infections or superinfection (53). Superinfections exacerbate the proinflammatory environment of common viral infections and are associated with increased morbidity and mortality (53,54). To our surprise, HSPC infusion was protective in a model of influenza and GAS superinfection, suggesting that its protective effects are robust even the setting of severe inflammation. In our mouse models, infection dramatically increased cytokine levels within just three days of infection. Interestingly, HSPC infusion was accompanied by an overall decrease in serum cytokine levels and a specific dampening of cytokines involved in "cytokine storm" (5,51,52). HSPCs have been described to produce cytokines, indicating that they have the capacity to direct immune function (55). However, whether the cytokines produced by HSPCs themselves contribute to the regulation of the immune response has heretofore been unknown. Our data point toward an immunomodulatory role of HSPC infusion that could prevent immune dysregulation during sepsis.

Immunoregulatory cells in the hematopoietic system include Tregs, Bregs, and MDSCs (47,49,56). Perhaps the most recognized immunomodulatory cell known is the Treg. While Tregs have essential roles regulating immune responses to pathogens (47), we did not see differences in any lymphocyte population, including T cells, that would suggest a Treg-mediated anti-inflammatory mechanism after HSPC infusion. MDSCs are immature myeloid cells that have strong anti-inflammatory roles by suppressing the responses of T-helper cells that contribute to the development of sepsis (49,57,58). PMN-MDSCs and M-MDSCs have strong anti-inflammatory functions that can be beneficial or detrimental depending on the setting. In fact,

some studies have shown that MDSCs contribute to clinical worsening during sepsis (49). For almost three decades, increased circulating immature myeloid cells have been a clinical marker of SIRS (59). Interestingly, increased MDSCs during sepsis have also been associated with increased development of nosocomial infections (56). However, in our GAS model of accelerated infection, the increase in MDSC populations after HSPC infusion was accompanied by lower overall cytokine levels and increased survival, suggesting that the immunomodulatory functions of MDSCs are beneficial during the early stages of systemic inflammation and could prevent sepsis-related mortality (60).

An important limitation of our study is that the lineage fate and the tissue or organ destination of the infused HSPCs at the early stages of infusion remain unknown. The small number of cells infused makes it challenging to identify them in the pool of endogenous cells of the recipient mice. While our data suggest that infused HSPCs directly and indirectly boost MDSC production by endogenous cells, further work will be required to determine the mechanisms by which HSPCs contribute to MDSC expansion. In addition, further analysis of HSPC subpopulations will be required to determine if long term HSCs or short-lived multipotent progenitors confer the greatest therapeutic potential. Identifying a short-lived hematopoietic progenitor that can signal endogenous cells to restore MDSC populations could represent a promising alternative therapeutic avenue (12,14,16) to treat sepsis while avoiding concern of possible graft versus host disease complications (61,62).

Currently, G-CSF, GM-CSF, and granulocyte transfusion (13,42,63) are used to prevent or treat sepsis in oncology patients with chemotherapy-induced fever and neutropenia. However, the clinical efficacy of granulocyte transfusion is poor (42,63). Here, we have shown infusing HSPCs is a promising alternative to granulocyte transfusion. Current granulocyte doses in humans are around $1x10^{10}$ cells per m^2 body surface area given daily or every other day (42,64). Our infusion model only uses a single dose of $1.7x10^7$ cells per m^2 body surface area (or 10,000

HSPCs in a mouse). It is important to emphasize that 10,000 HSPCs is a relatively small number of cells to infuse into a mouse as it represents less than 0.01% of the nucleated bone marrow cells in a mouse. Collectively, the single low HSPC dose compared to multiple larger granulocyte transfusions suggests that HSPCs are more effective than granulocytes, cell for cell, in the treatment of sepsis. Our findings could lead to the development of an efficacious new therapeutic approach that could succeed where granulocyte infusions have fallen short.

Materials and Methods

Mice

We used WT C57Bl/6 (CD45.2) and C57Bl/6.SJL (CD45.1) mice 8–10 weeks of age. Lineage tracing using KRT18-CreERT2 : Rosa26-lox-STOP-lox-TdTomato we made by crossing KRT18-CreERT2 mice obtained from Dr. Daisuke Nakada (Baylor College of Medicine) and Rosa26-lox-STOP-lox-TdTomato mice (stock # 007914) obtained from Jackson Laboratories (Bar Harbor, ME USA, www.jax.org). All mice genotypes were confirmed by polymerase chain reaction (PCR) prior to the start of the experiments. Mice were assigned to each experimental group at random. Both male and female mice were used for all the experiments except for the superinfection survival studies as it has been shown that female mice have long-lasting hyperresponsiveness to respiratory infections (65). Therefore, only male mice were used in the superinfection experiments. Individual mice were assigned to groups randomly and were age and sex matched for each independent experiment.

Pathogen inoculation and quantification

Mice were infected with *Streptococcus pyogenes* strain MGAS315 by intramuscular injection on the hind limb with $2x10^6$ CFU. To determine the bacterial load, limb, spleen, and blood were collected from infected mice. Limb and spleen tissue were homogenized, serially diluted, and plated on blood agar plates (BAP) (BD, Franklyn Lake, New Jersey, www.bd.com). Blood was serially diluted and plated on BAP. Limb and spleen bacterial load was normalized to the grams of tissue that was homogenized.

Influenza A H1N1 PR8 strain infections were done by intranasal inoculation with 150 PFU. Viral load was quantified by collecting viral particles from lung lavage fluid using Amicon Ultra 0.5 mL (Millipore Sigma, Burlington Massachusetts. www.emdmillipore.com), and RNA was purified

using the TRIZOL method followed by the quantification of viral particles by Real-Time PCR of virus-specific nucleoprotein (NP) gene. The exact quantity was calculated using a standard curve of purified viral particles with known concentration and normalized by the amount of lung tissue collected.

Flow cytometry and cell sorting

Flow cytometry analyses were done using LSR II and BD Fortessa instruments. Cells were identified by the differential expression of markers listed in **Supplemental Table 1.** Our cocktail of Lineage (Lin) markers include Gr1, CD11b, B220, CD4, CD8, and Ter119.

Cell sorting of HSPCs and their subpopulations were done using the SONY SH800 sorter and the BD FACS Aria Fusion using the markers listed in **Supplemental Table 1**. Post-sort purity test showed that sorted cells were 95-98% pure.

Cre induction

Cre activation in KRT18-CreERT2 : Rosa26-lox-STOP-lox-TdTomato was induced with Tamoxifen. Each mouse was administered tamoxifen by intraperitoneal injection at a dose of 100mg/Kg body weight for five consecutive days prior to the start of the lineage tracing experiments.

Cell infusion

All infusions were done intravenously by retroorbital injection. Rescued mice received cells resuspended in saline solution while the control mice were injected with saline solution alone.

Cytokine profiling

Serum was collected using a BD Microtainer blood collection tube (San Jose, CA. www.bdbiosciences.com). Serum levels of cytokines were analyzed through Eve Technologies company (Calgary, AB, Canada. www.evetechnologies.com).

T cell suppression assay

T cells were isolated from the spleen using anti-CD3 magnetic beads from Miltenyi Biotec (Bergisch Gladbach, Germany. www.miltenyibiotec.com) and MDSCs were sorted using the SONY SH800 sorter and the BD FACS Aria Fusion as described above. T cell were activated with anti-CD3 and anti-CD28 coated plates and supplemented with IL-2 to support proliferation and then cultured alone of with M-MDSCs or PMN-MDSCs. T cells were stained with CellTrace Violet and proliferation mas measured by dye dilution using flow cytometry.

Statistical tests

Normality was assessed using the Shapiro-Wilk test and variances were compared using F-tests. Comparisons between two groups were made done using unpaired *t*-test for parametric data, Welch's *t*-test for parametric data without equal variances, and Mann-Whitney test for non-parametric data. Tests involving three or more comparisons we done using One Way ANOVA with Tukey's correction for multiple comparisons or Kruskal-Wallis test with Dunn's correction for multiple comparisons. Comparisons of survival curves were done using Mantel-Cox tests. Outliers were identified using the ROUT method (Q=5%). Graphs are shown as Mean +/- SEM. Sample size of each experiment was calculated based on pilot experiments and using an alpha=0.05 and power=0.80. Each specific statistical test used as well as group size and independent experiments are described on each figure legend.

Study approval

Mice are housed in AAALAC-accredited, specific-pathogen-free animal facilities at Baylor College of Medicine and Texas Children's Hospital. All experiments are approved and follow the guidelines stated in our protocol approved by the Institutional Animal Care and Use Committee (IACUC) and by the Baylor College of Medicine institutional review board.

Author contributions

DEMM performed and designed the experiments shown in the study and conducted the data analysis. ARF, and SP assisted in designing the superinfection model involving influenza and GAS pathogens. DL and BK assisted with intranasal influenza infections. KYK directed the project and participated in all aspects of experimental design, data analysis and interpretation. DEMM and KYK wrote the article, and all authors discussed and commented during the writing of the manuscript.

Acknowledgements

The authors would like to thank Catherine Gillespie, Maksim Mamonkin, Meghan Kisiel, Olumide Ayeni, and members of the King lab for their input into the study. DEMM and KYK were supported by the NIH grants R01HL136333, R01HL134880, and R35HL155672 (KYK). DEMM was also supported by the Howard Hughes Medical Institute (HHMI) Gilliam Fellowship for Advanced Study. This project was supported by the Cytometry and Cell Sorting Core at Baylor College of Medicine with funding from the CPRIT Core Facility Support Award (CPRIT-RP180672), the NIH (CA125123 and RR024574), and the assistance of Joel M. Sederstrom. This project was also assisted by the Dan L. Duncan Cancer Center and the William T. Shearer Center for Human Immunobiology.

Conflict of interest statement

The authors have declared that there are no conflicts of interest.

References

1. Rhee C, Jones TM, Hamad Y, et al. Prevalence, Underlying Causes, and Preventability of Sepsis-Associated Mortality in US Acute Care Hospitals. *JAMA Network Open*. 2019;2(2):1-14. doi:10.1001/jamanetworkopen.2018.7571
2. Van Der Poll T, Van De Veerdonk FL, Scicluna BP, Netea MG. The immunopathology of sepsis and potential therapeutic targets. *Nature Reviews Immunology*. 2017;17:407-420. doi:10.1038/nri.2017.36
3. Deutschman CS, Tracey KJ. Sepsis: Current dogma and new perspectives. *Immunity*. 2014;40(4):463-475. doi:10.1016/j.immuni.2014.04.001
4. Yu X, Zhang X, Zhao B, et al. Intensive cytokine induction in pandemic H1N1 influenza virus infection accompanied by robust production of IL-10 and IL-6. *PLoS ONE*. 2011;6(12):1-9. doi:10.1371/journal.pone.0028680
5. Huang KJ, Su IJ, Theron M, et al. An interferon-γ-related cytokine storm in SARS patients. *Journal of Medical Virology*. 2005;75(2):185-194. doi:10.1002/jmv.20255
6. Wang SM, Lu IH, Lin YL, et al. The severity of Streptococcus pyogenes infections in children is significantly associated with plasma levels of inflammatory cytokines. *Diagnostic Microbiology and Infectious Disease*. 2008;61(2):165-169. doi:10.1016/j.diagmicrobio.2008.01.008
7. Napolitano LM. Sepsis 2018: Definitions and Guideline Changes. *Surgical Infections*. 2018;19(2):117-125. doi:10.1089/sur.2017.278
8. Krebs J, Hillenbrand A, Tsagogiorgas C, et al. Intravenous delivery of granulocyte-macrophage colony stimulating factor impairs survival in lipopolysaccharide-induced sepsis. *PLoS ONE*. 2019;14(6):1-14. doi:10.1371/journal.pone.0218602
9. Estcourt LJ, Stanworth S, Doree C, et al. Granulocyte transfusions for preventing infections in people with neutropenia or neutrophil dysfunction. *Cochrane Database of Systematic Reviews*. 2016;2016(4). doi:10.1002/14651858.CD005339.pub2
10. Li Y, Yang S, Wang G, et al. Effects of immunotherapy on mortality in neonates with suspected or proven sepsis: a systematic review and network meta-analysis. *BMC Pediatrics*. 2019;19(270):1-10. doi:10.1186/s12887-019-1609-1
11. Mathias B, Szpila BE, Moore FA, Efron PA, Moldawer LL. A Review of GM-CSF Therapy in Sepsis. *Medicine*. 2015;94(50):1-10. doi:10.1097/MD.0000000000002044
12. Hidalgo A, Chilvers ER, Summers C, Koenderman L. The Neutrophil Life Cycle. *Trends in Immunology*. 2019;40(7). doi:10.1016/j.it.2019.04.013
13. Robinson SP, Marks DI. Granulocyte transfusions in the G-CSF era. Where do we stand? *Bone Marrow Transplantation*. Published online 2004. doi:10.1038/sj.bmt.1704630
14. Karpova D, Ritchey J, Holt M, et al. Continuous blockade of CXCR4 results in dramatic mobilization and expansion of hematopoietic stem and progenitor cells. *Blood*. 2017;129:2939-2949. doi:10.1182/blood-2016-10-746909
15. Burberry A, Zeng MY, Ding L, et al. Infection mobilizes hematopoietic stem cells through cooperative NOD-like receptor and toll-like receptor signaling. *Cell Host and Microbe*. 2014;15(6):779-791. doi:10.1016/j.chom.2014.05.004
16. Nagai Y, Garrett KP, Ohta S, et al. Toll-like Receptors on Hematopoietic Progenitor Cells Stimulate Innate Immune System Replenishment. *Immunity*. 2006;24(6):801-812. doi:10.1016/j.immuni.2006.04.008
17. Schürch CM, Riether C, Ochsenbein AF. Cytotoxic CD8+ T cells stimulate hematopoietic progenitors by promoting cytokine release from bone marrow mesenchymal stromal cells. *Cell Stem Cell*. 2014;14(4):460-472. doi:10.1016/j.stem.2014.01.002

18. Matatall KA, Shen CC, Challen GA, King KY. Type II interferon promotes differentiation of myeloid-biased hematopoietic stem cells. *Stem Cells*. 2014;32(11):3023-3030. doi:10.1002/stem.1799
19. Baldridge MT, King KY, Goodell MA. Inflammatory signals regulate hematopoietic stem cells. *Trends in Immunology*. 2011;32(2):57-65. doi:10.1016/j.it.2010.12.003
20. Pietras EM, Mirantes-Barbeito C, Fong S, et al. Chronic interleukin-1 exposure drives haematopoietic stem cells towards precocious myeloid differentiation at the expense of self-renewal. *Nature Cell Biology*. 2016;18(6):607-618. doi:10.1038/ncb3346
21. Takizawa H, Fritsch K, Kovtonyuk L V., et al. Pathogen-Induced TLR4-TRIF Innate Immune Signaling in Hematopoietic Stem Cells Promotes Proliferation but Reduces Competitive Fitness. *Cell Stem Cell*. 2017;21(2):225-240.e5. doi:10.1016/j.stem.2017.06.013
22. Morales-Mantilla DE, King KY. The Role of Interferon-Gamma in Hematopoietic Stem Cell Development , Homeostasis , and Disease. *Current Stem Cell Reports*. 2018;4(3):264-271. doi:10.1007/s40778-018-0139-3
23. Chambers SM, Boles NC, Lin KYK, et al. Hematopoietic Fingerprints: An Expression Database of Stem Cells and Their Progeny. *Cell Stem Cell*. 2007;1(5):578-591. doi:10.1016/j.stem.2007.10.003
24. Sun J, Ramos A, Chapman B, et al. Clonal dynamics of native haematopoiesis. *Nature*. 2014;514(7522):322-327. doi:10.1038/nature13824
25. Rodriguez-Fraticelli AE, Wolock SL, Weinreb CS, et al. Clonal analysis of lineage fate in native haematopoiesis. *Nature*. 2018;553(7687):212-216. doi:10.1038/nature25168
26. Cabezas-Wallscheid N, Klimmeck D, Hansson J, et al. Identification of regulatory networks in HSCs and their immediate progeny via integrated proteome, transcriptome, and DNA methylome analysis. *Cell Stem Cell*. 2014;15(4):507-522. doi:10.1016/j.stem.2014.07.005
27. MacNamara KC, Oduro K, Martin O, et al. Infection-Induced Myelopoiesis during Intracellular Bacterial Infection Is Critically Dependent upon IFN-γ Signaling. *The Journal of Immunology*. 2011;186(2):1032-1043. doi:10.4049/jimmunol.1001893
28. Matatall KA, Jeong M, Chen S, et al. Chronic Infection Depletes Hematopoietic Stem Cells through Stress-Induced Terminal Differentiation. *Cell Reports*. 2016;17(10):2584-2595. doi:10.1016/j.celrep.2016.11.031
29. Sato A, Kamio N, Yokota A, et al. C/EBPβ isoforms sequentially regulate regenerating mouse hematopoietic stem/progenitor cells. *Blood Advances*. 2020;4(14):3343-3356. doi:10.1182/bloodadvances.2018022913
30. Efstratiou A, Lamagni T. Epidemiology of Streptococcus pyogenes. In: *Streptococcus Pyogenes : Basic Biology to Clinical Manifestations*. Vol 3. ; 2016.
31. Emgård J, Bergsten H, Mccormick JK, et al. MAIT Cells Are Major Contributors to the Cytokine Response in Group A Streptococcal Toxic Shock Syndrome. *Nature Scientific Reports*. 2019;7:1-9. doi:10.1073/pnas.1910883116
32. Walker MJ, Barnett TC, Mcarthur JD, et al. Disease Manifestation and pathogenic Mechanism of Group A Streptococcus. *Clinical Microbiology Reviews*. 2014;27(2):264-301. doi:10.1128/CMR.00101-13
33. Gong T, Liu L, Jiang W, Zhou R. DAMP-sensing receptors in sterile inflammation and inflammatory diseases. *Nature Reviews Immunology*. 2020;20(2):95-112. doi:10.1038/s41577-019-0215-7
34. Esplin BL, Shimazu T, Welner RS, et al. Chronic Exposure to a TLR Ligand Injures Hematopoietic Stem Cells. *The Journal of Immunology*. 2011;186(9):5367-5375. doi:10.4049/jimmunol.1003438

35. Chou DB, Sworder B, Bouladoux N, et al. Stromal-derived IL-6 alters the balance of myeloerythroid progenitors during Toxoplasma gondii infection. *Journal of leukocyte biology*. 2012;92(1):123-131. doi:10.1189/jlb.1011527
36. Tsou CL, Peters W, Si Y, et al. Critical roles for CCR2 and MCP-3 in monocyte mobilization from bone marrow and recruitment to inflammatory sites. *Journal of Clinical Investigation*. 2007;117(4):902-909. doi:10.1172/JCI29919
37. Schultze JL, Mass E, Schlitzer A. Emerging Principles in Myelopoiesis at Homeostasis and during Infection and Inflammation. *Immunity*. 2019;50(2):288-301. doi:10.1016/j.immuni.2019.01.019
38. Yang X, Chen D, Long H, Zhu B. The mechanisms of pathological extramedullary hematopoiesis in diseases. *Cellular and Molecular Life Sciences*. 2020;77(14):2723-2738. doi:10.1007/s00018-020-03450-w
39. Baldridge MT, King KY, Boles NC, Weksberg DC, Goodell MA. Quiescent haematopoietic stem cells are activated by IFN-γ in response to chronic infection. *Nature*. 2010;465:793-797. doi:10.1038/nature09135
40. Chapple RH, Tseng YJ, Hu T, et al. Lineage tracing of murine adult hematopoietic stem cells reveals active contribution to steady-state hematopoiesis. *Blood Advances*. 2018;2(11):1220-1228. doi:10.1182/bloodadvances.2018016295
41. Gekas C, Graf T. CD41 expression marks myeloid-biased adult hematopoietic stem cells and increases with age. *Blood*. 2013;121(22):4463-4472. doi:10.1182/blood-2012-09-457929
42. Price TH, Boeckh M, Harrison RW, et al. Efficacy of transfusion with granulocytes from G-CSF / dexamethasone – treated donors in neutropenic patients with infection. *Blood*. 2015;126(18):2153-2162. doi:10.1182/blood-2015-05-645986.Presented
43. Baccam P, Beauchemin C, Macken CA, Hayden FG, Perelson AS. Kinetics of Influenza A Virus Infection in Humans. *Journal of Virology*. 2006;80(15):7590-7599. doi:10.1128/jvi.01623-05
44. Smith AM, Perelson AS. Influenza A virus infection kinetics: Quantitative Data and Models. *Wiley Interdisciplinary Reviews: Systems Biology and Medicine*. 2011;3(4):429-445. doi:10.1002/wsbm.129.
45. Jaffer U, Wade RG, Gourlay T. Cytokines in the systemic inflammatory response syndrome: a review. *HSR Proceedings*. 2010;2:161-175.
46. Skirecki T, Mikaszewska-Sokolewicz M, Godlewska M, et al. Mobilization of Stem and Progenitor Cells in Septic Shock Patients. *Scientific Reports*. 2019;9. doi:10.1038/s41598-019-39772-4
47. Maizels RM, Smith KA. *Regulatory T Cells in Infection*. Vol 112.; 2011. doi:10.1016/B978-0-12-387827-4.00003-6
48. Rosser EC, Mauri C. Regulatory B Cells: Origin, Phenotype, and Function. *Immunity*. 2015;42:607-612. doi:10.1016/j.immuni.2015.04.005
49. Schrijver IT, Théroude C, Roger T. Myeloid derived suppressor cells in sepsis. *Frontiers in Immunology*. 2019;10:1-10. doi:10.3389/fimmu.2019.00327
50. Frank K, Paust S. Dynamic Natural Killer Cell and T Cell Responses to Influenza Infection. *Frontiers in Cellular and Infection Microbiology*. 2020;10:1-21. doi:10.3389/fcimb.2020.00425
51. Karki R, Sharma BR, Tuladhar S, et al. Synergism of TNF- a and IFN- g Triggers Inflammatory Cell Death , Tissue Damage , and Mortality in SARS- CoV-2 Infection and Cytokine Shock Syndromes. *Cell*. 2021;184:149-168. doi:https://doi.org/10.1016/j.cell.2020.11.025
52. Fajgenbaum DC, June CH. Cytokine Storm. *New England Journal of Medicine*. 2020;383(23):2255-2273. doi:10.1056/nejmra2026131

53. Rynda-Apple A, Robinson KM, Alcorn JF. Influenza and bacterial superinfection: Illuminating the immunologic mechanisms of disease. *Infection and Immunity*. 2015;83(10):3764-3770. doi:10.1128/IAI.00298-15
54. Paget C, Trottein F. Mechanisms of bacterial superinfection post-influenza: A role for unconventional T cells. *Frontiers in Immunology*. 2019;10:1-13. doi:10.3389/fimmu.2019.00336
55. Chen CI, Zhang L, Datta SK. Hematopoietic stem and multipotent progenitor cells produce IL-17, IL-21 and other cytokines in response to TLR signals associated with late apoptotic products and augment memory Th17 and Tc17 cells in the bone marrow of normal and lupus mice. *Clinical Immunology*. 2016;162:9-26. doi:10.1016/j.clim.2015.10.007
56. Uhel F, Azzaoui I, Grégoire M, et al. Early expansion of circulating granulocytic myeloid-derived suppressor cells predicts development of nosocomial infections in patients with sepsis. *American Journal of Respiratory and Critical Care Medicine*. 2017;196(3):315-327. doi:10.1164/rccm.201606-1143OC
57. Köstlin N, Vogelmann M, Spring B, et al. Granulocytic myeloid-derived suppressor cells from human cord blood modulate T-helper cell response towards an anti-inflammatory phenotype. *Immunology*. 2017;152:89-101. doi:10.1111/imm.12751
58. Delano MJ, Scumpia PO, Weinstein JS, et al. MyD88-dependent expansion of an immature GR-1 +CD11b+ population induces T cell suppression and Th2 polarization in sepsis. *Journal of Experimental Medicine*. 2007;204(6):1463-1474. doi:10.1084/jem.20062602
59. Bone RC, Balk RA, Cerra FB, et al. Definitions for sepsis and organ failure and guidelines for the use of innovative therapies in sepsis. *Chest*. 1992;101(6):1644-1655. doi:10.1378/chest.101.6.1644
60. Marriott I, Li J, Gottlieb Land W, et al. Taurodeoxycholate Increases the Number of Myeloid-Derived Suppressor Cells That Ameliorate Sepsis in Mice. *Frontiers in Immunology | www.frontiersin.org*. 2018;9. doi:10.3389/fimmu.2018.01984
61. Batsali AK, Georgopoulou A, Mavroudi I, Matheakakis A, Pontikoglou CG, Papadaki HA. The Role of Bone Marrow Mesenchymal Stem Cell Derived Extracellular Vesicles (MSC-EVs) in Normal and Abnormal Hematopoiesis and Their Therapeutic Potential. *Journal of Clinical Medicine*. 2020;9(856):1-14. doi:10.3390/jcm9030856
62. Tijaro-Ovalle NM, Karantanos T, Wang HT, Boussiotis VA. Metabolic targets for improvement of allogeneic hematopoietic stem cell transplantation and graft-vs.host disease. *Frontiers in Immunology*. 2019;10(295):1-13. doi:10.3389/fimmu.2019.00295
63. Klein K, Castillo B. Historical perspectives, current status, and ethical issues in granulocyte transfusion. *Annals of Clinical and Laboratory Science*. 2017;47(4):501-507.
64. Teofili L, Valentini CG, di Blasi R, et al. Dose-dependent effect of granulocyte transfusions in hematological patients with febrile neutropenia. *PLoS ONE*. 2016;11(8):1-15. doi:10.1371/journal.pone.0159569
65. Larcombe AN, Foong RE, Bozanich EM, et al. Sexual dimorphism in lung function responses to acute influenza A infection. *Influenza and other Respiratory Viruses*. 2011;5(5):334-342. doi:10.1111/j.1750-2659.2011.00236.x

Figures and figure legends

Figure 1

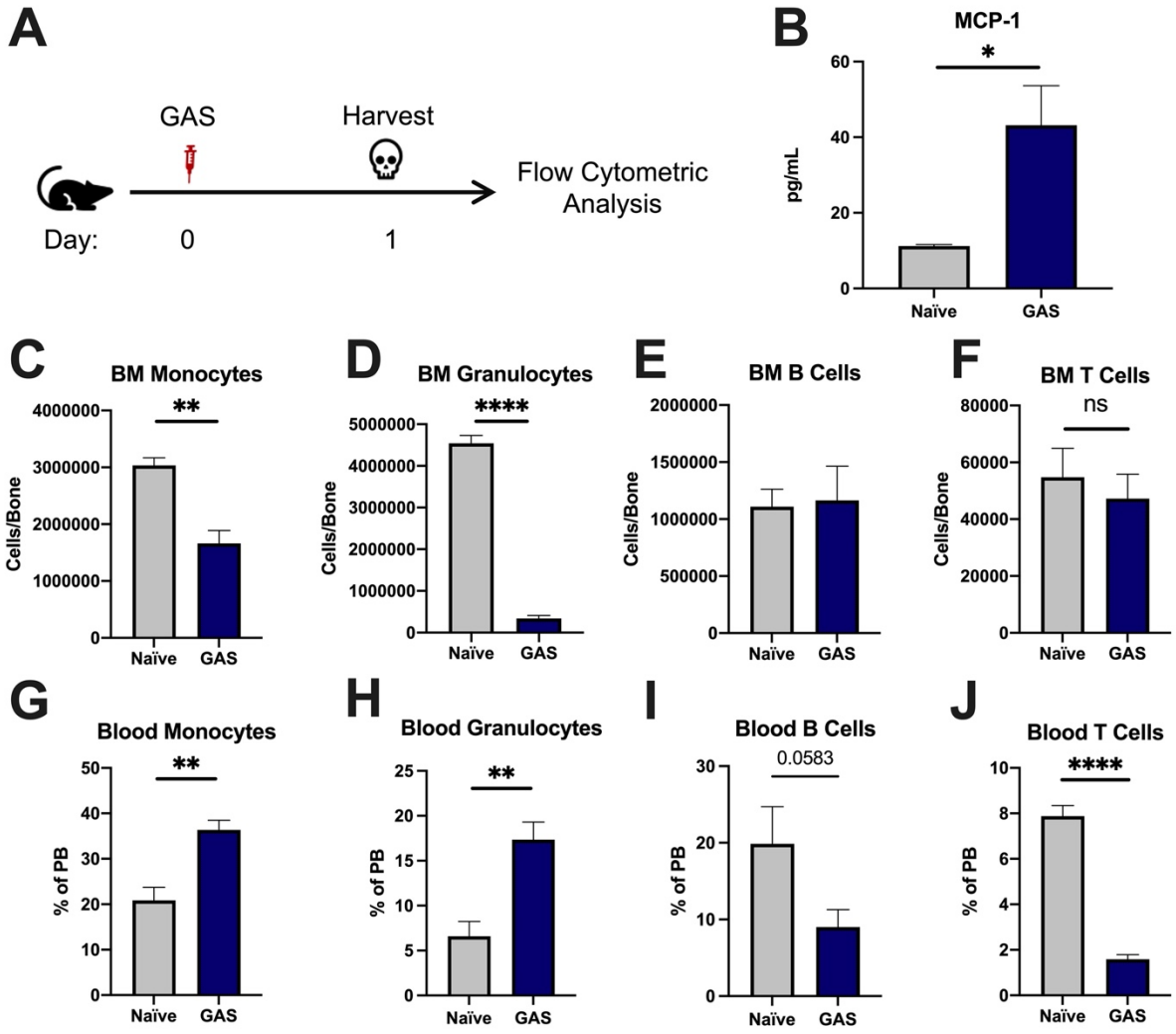

Figure 1. GAS infection promotes a rapid myeloid cell response. (A) Experimental time frame of GAS infection and BM analysis. (B) Serum levels of MCP-1 of naïve and GAS-infected mice. Absolute number of (C) monocytes, (D) granulocytes, (E) B cells, and (F) F cells in the BM of naïve and infected mice. Relative abundance of (G) monocytes, (H) granulocytes, (I) B cells, and (J) T cells in the blood. (B-J) Data is representative of 3 independent experiments; n = 3-5 mice/group; Statistical comparison done using Unpaired t-test; *p<0.05, **p<0.01, ****p<0.0001. Outliers were identified using the ROUT method (Q=5%).

Figure 2

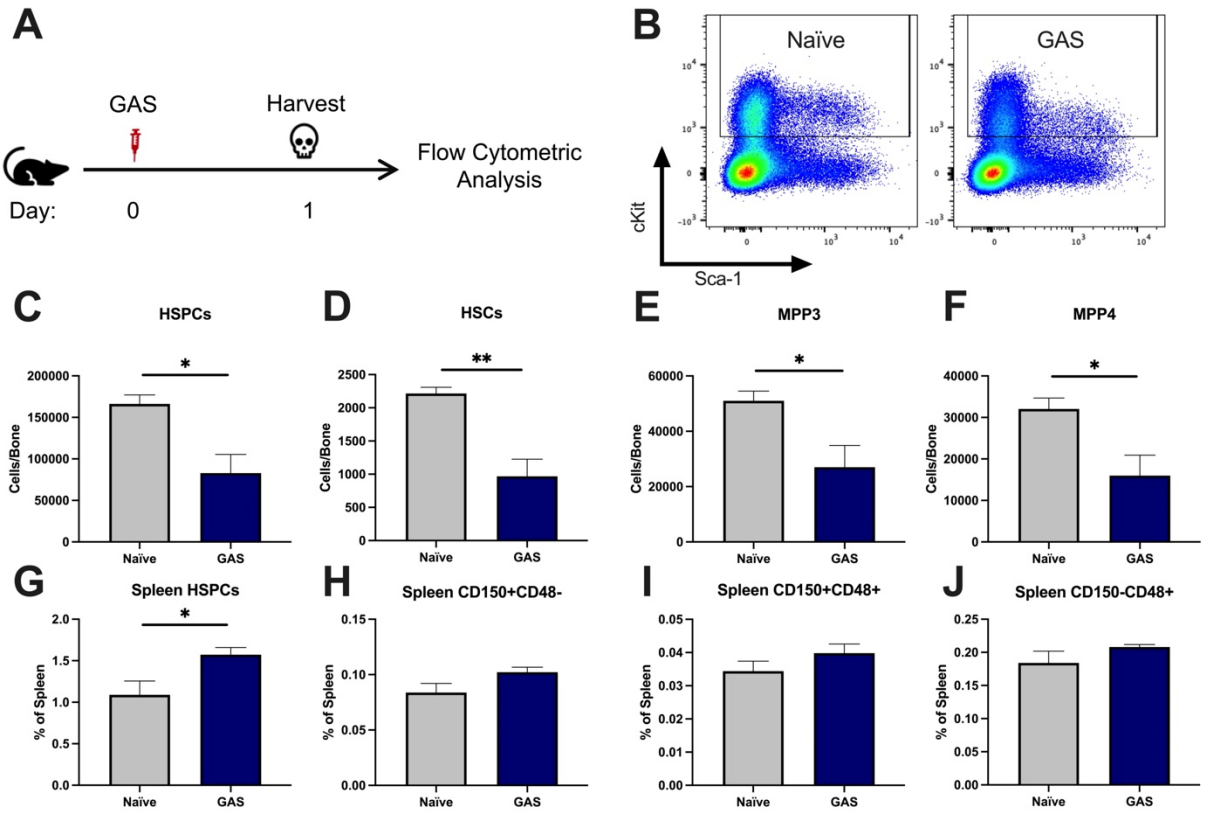

Figure 2. GAS infection depletes BM HSPCs 24hrs post infection. (A) Experimental time frame of GAS infection and BM analysis. (B) Flow plot of HSPC gating and representation of different surface expression of cKit and Sca-1 during infection. Plots are gated from lineage negative BM cells. (C-F) Absolute number of HSPCs, HSCs, multipotent progenitors (MPP) 3, and MPP4 in the BM of naïve and GAS infected mice. Spleen populations of (G) HSPCs, (H) HSC/MPP1, (I) MPP2, and (J) MMP3/4 identified by differential expression of CD150 and CD48. (C-J) Data is representative of 3 independent experiments; n = 4-5 mice/group; Statistical comparison done using Unpaired t-test; *p<0.05, **p<0.01. Outliers were identified using the ROUT method (Q=5%).

Figure 3

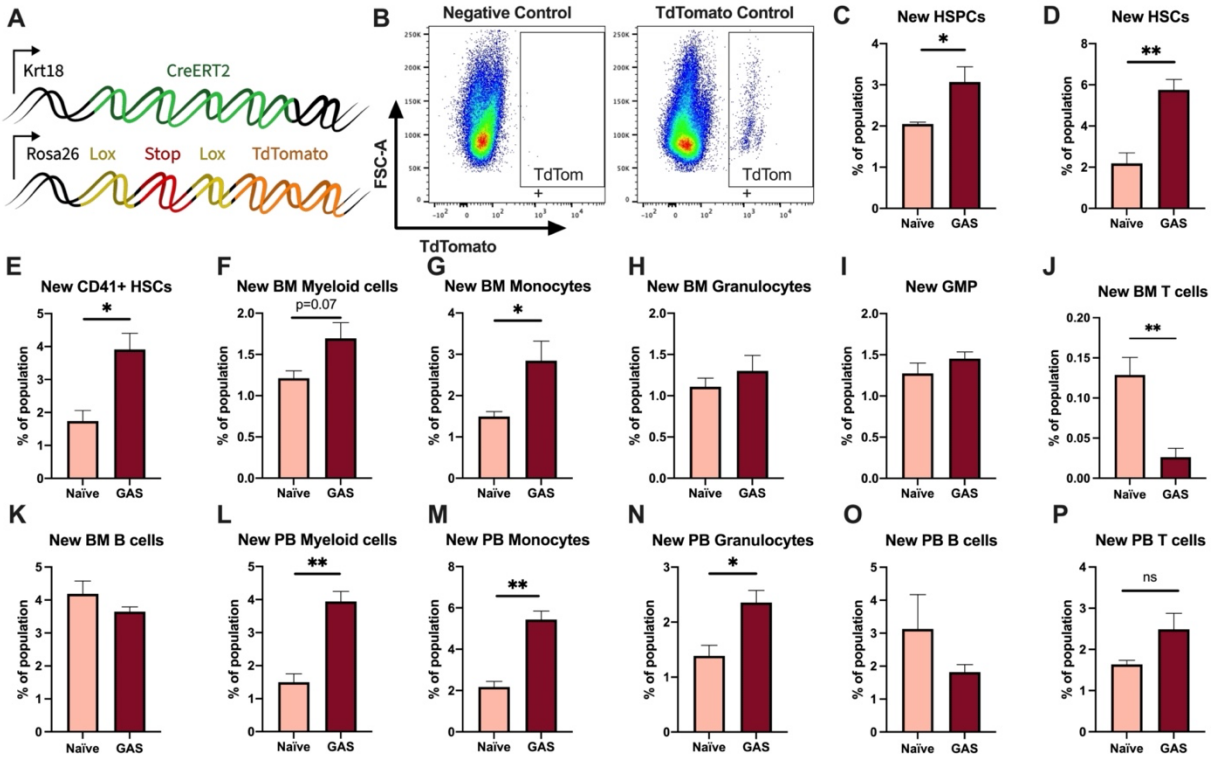

Figure 3. Krt18 lineage tracing of naïve and GAS-infected HSCs. (A) Genetic model of KRT18-CreERT2:Rosa26-lox-STOP-lox-TdTomato mouse system. (B) Representative gating of TdTomato expression in negative control (left; Genotype: Krt18-CreERT2^{+}) and Tamoxifen-induced positive control (right: Genotype: KRT18-CreERT2^{+} : Rosa26-lox-STOP-lox-TdTomato$^{+/-}$). Percent of BM (C) HSPC, (D) HSC, (E) CD41+ HSC, and (F) myeloid populations that are TdTomato+. Percent of BM (G) total monocytes, (H) granulocytes, (I) GMP, (J) BM T cells, and (K) BM B cells that are TdTomato+. Percent of PB (L) total myeloid cells, (M) monocytes, (N) granulocytes, (O) T cells, and (P) B cells that are TdTomato+. Data representative of 3 independent experiments; (C-N) n=5-7 mice/group. Statistical comparison done using Unpaired t-tests; *p<0.05, **p<0.01.

Figure 4

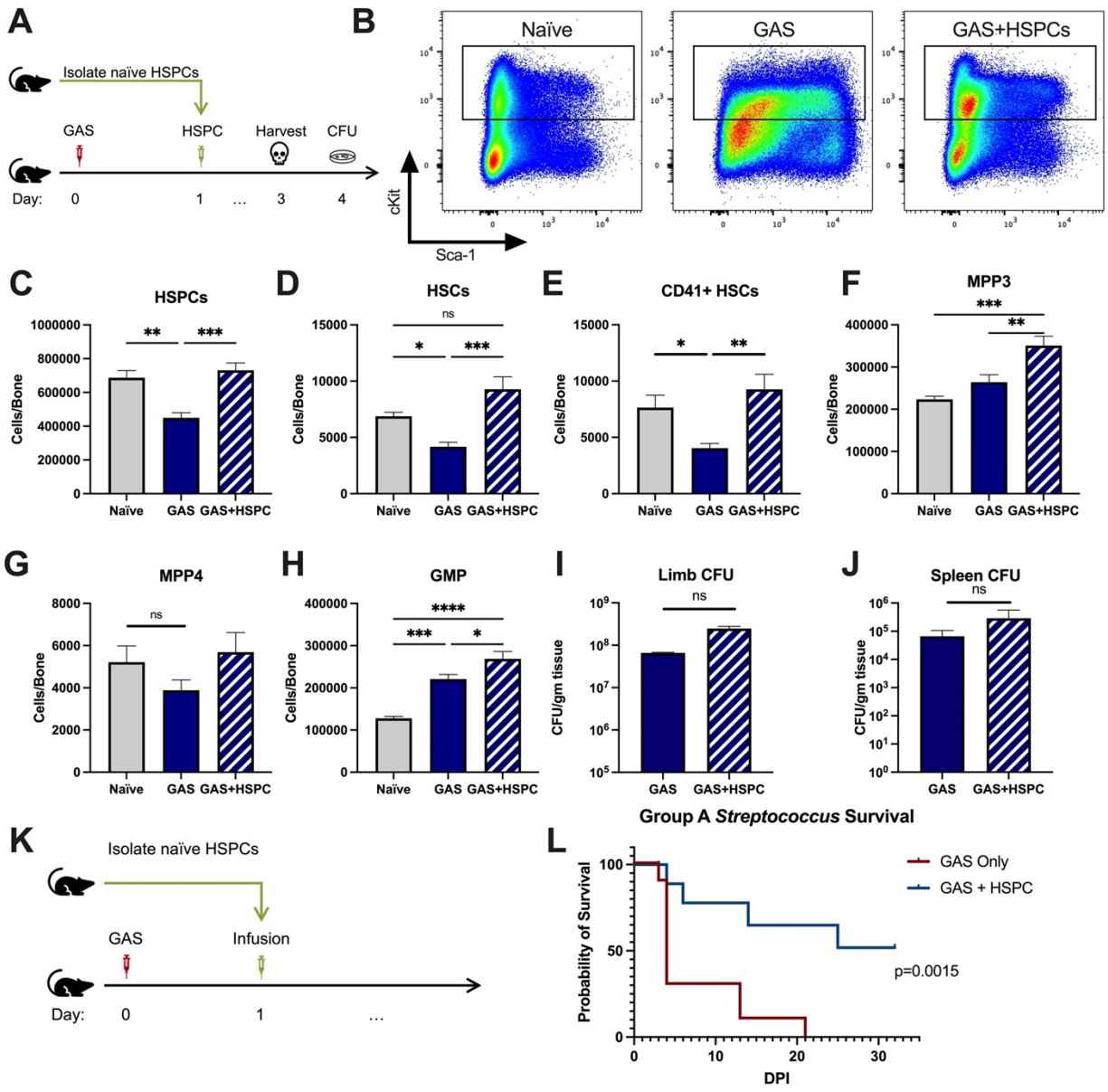

Figure 4. HSPC infusion in GAS-infected mice promotes survival and increases progenitor populations in the BM. (A) Experimental design of BM analysis and CFU count after HSPC infusion. (B) Flow plot of HSPC gating and representation of different surface expression of cKit and Sca-1 during infection. Plots are gated from lineage negative BM cells. (C-H) Absolute numbers of HSPCs, HSCs, and downstream progenitors in the BM of naïve, GAS-infected mice, and GAS-infected mice rescued with HSPCs. Quantified bacterial load in the (I) limb and (J) spleen of infected mice. (K) Experimental design of the survival study. (J) Survival curve of GAS infected mice with or without HSPC infusion. Data representative of 3 independent experiments; (C-H) n=5-7 mice/group, (I & J) n=8-10 mice/group, (L) n=9-10 mice/group. Statistical comparison done using (C-H) One-Way ANOVA with Tukey's correction for multiple comparisons or (I & J) Unpaired t-tests. ns=not significant, *p<0.05, **p<0.01, ***p<0.001 *****p<0.0001. Comparison of (L) survival was done using Log-rank (Mantel-Cox) test.

Figure 5

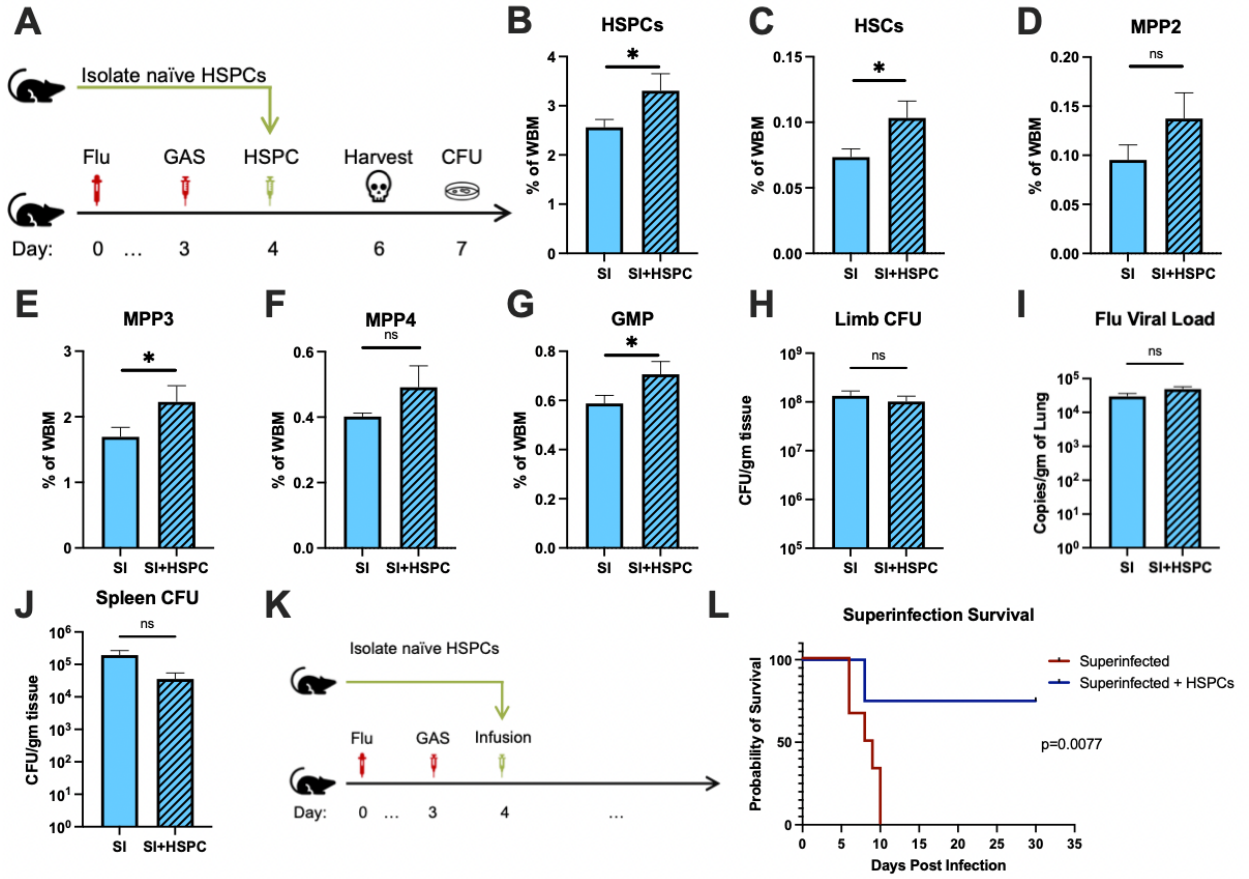

Figure 5. HSPC infusion in superinfected mice promotes survival without changing pathogen clearance. (A) Experimental design of BM analysis and CFU count post HSPC infusion in superinfected mice. (B-G) BM populations of HSPCs and downstream progenitors after HSPC infusion. Bacterial load in the (H) limb and (J) Spleen of infected mice. (I) Viral load of mice with or without HSPC infusion. (K) Experimental design of the survival studies on superinfected mice. (L) Survival curve after HSPC infusion. Experiments are representative of 3 independent experiments. (B-J) Comparison done with Unpaired t-test or Welch's *t*-test. (B-G) n=5, (H-J) n=9-11, and (L) n=9-10 mice per group. Comparison of (L) survival was done using Log-rank (Mantel-Cox) test. ns=not significant, *p<0.05.

Figure 6

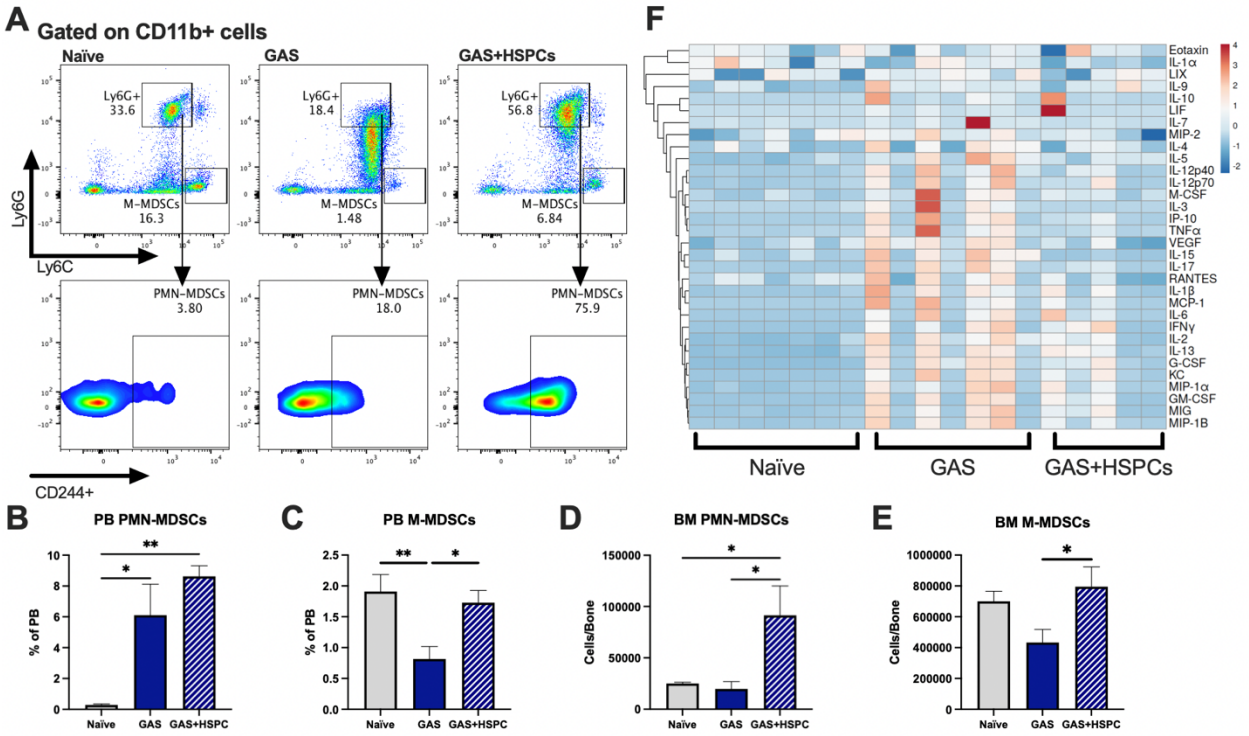

Figure 6. HSPC infusion increases and restores MDSC populations and dampends inflammation after GAS. (A) Representative gating of MDSCs by their surface expression of Ly6G and Ly6C. Gated on CD11b+ cells. PB populations of (B) PMN-MDSCs and (C) M-MDSCs of naïve, GAS-infected, and GAS-infected mice infused with HSPCs. BM populations of (D) PMN-MDSCs and (E) M-MDSCs of naïve, GAS-infected, and GAS-infected mice infused with HSPCs. (F) Heatmap of serum cytokine levels using ClustVis web tool (Metsalu and Vilo, 2015). Data representative of 2 (A-E) or 4 (F) independent experiments. (B-E) Statistical comparison done using One-Way ANOVA with Tukey's correction for multiple comparisons; n=7 mice per group; *p<0.05, **p<0.01. Outliers were identified using the ROUT method (Q=5%).

Figure 7

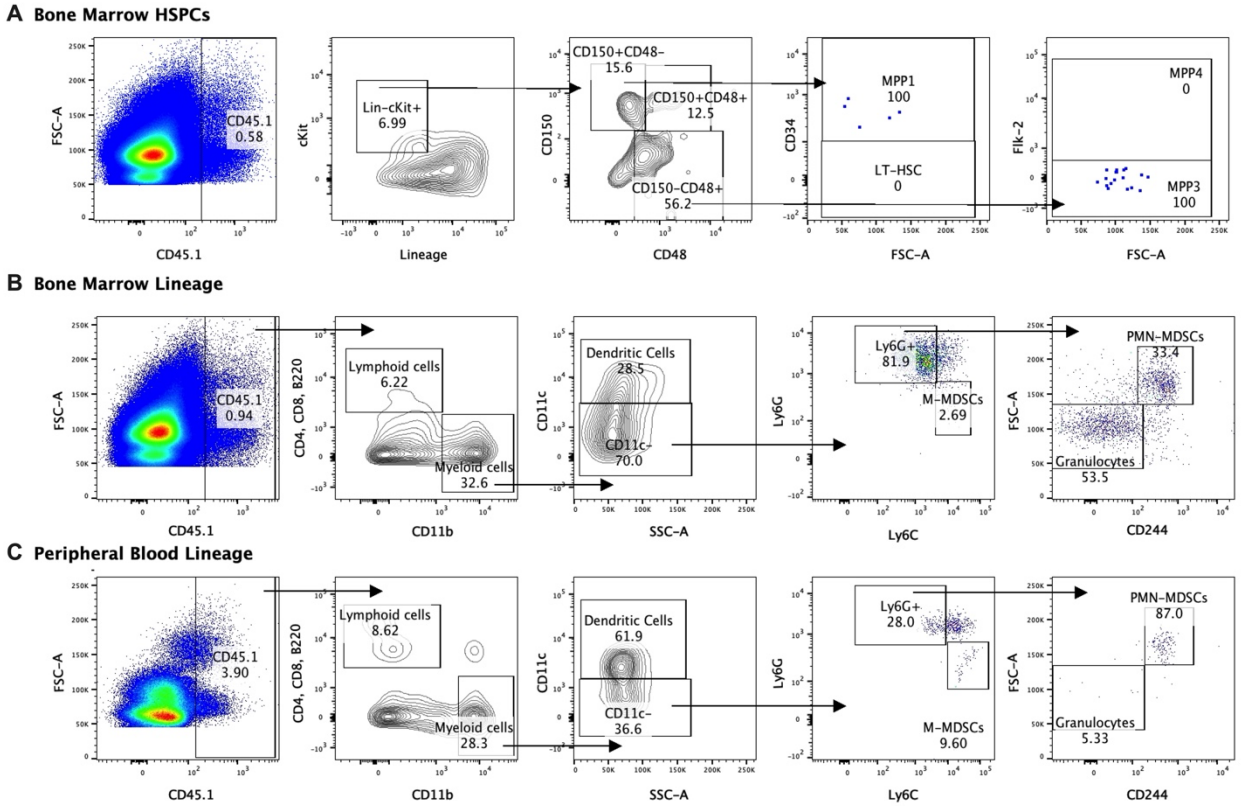

Figure 7. Lineage fate of infused HSPCs in GAS-infected mice skews myeloid without signs of stem cell engraftment. Gating representation of the lineage fate of (A) BM HSPCs, (B) BM lineage cells, and (C) PB lineage cells 30 days after GAS infection. Data is representative of 3 independent experiments.

Supplemental figure 1

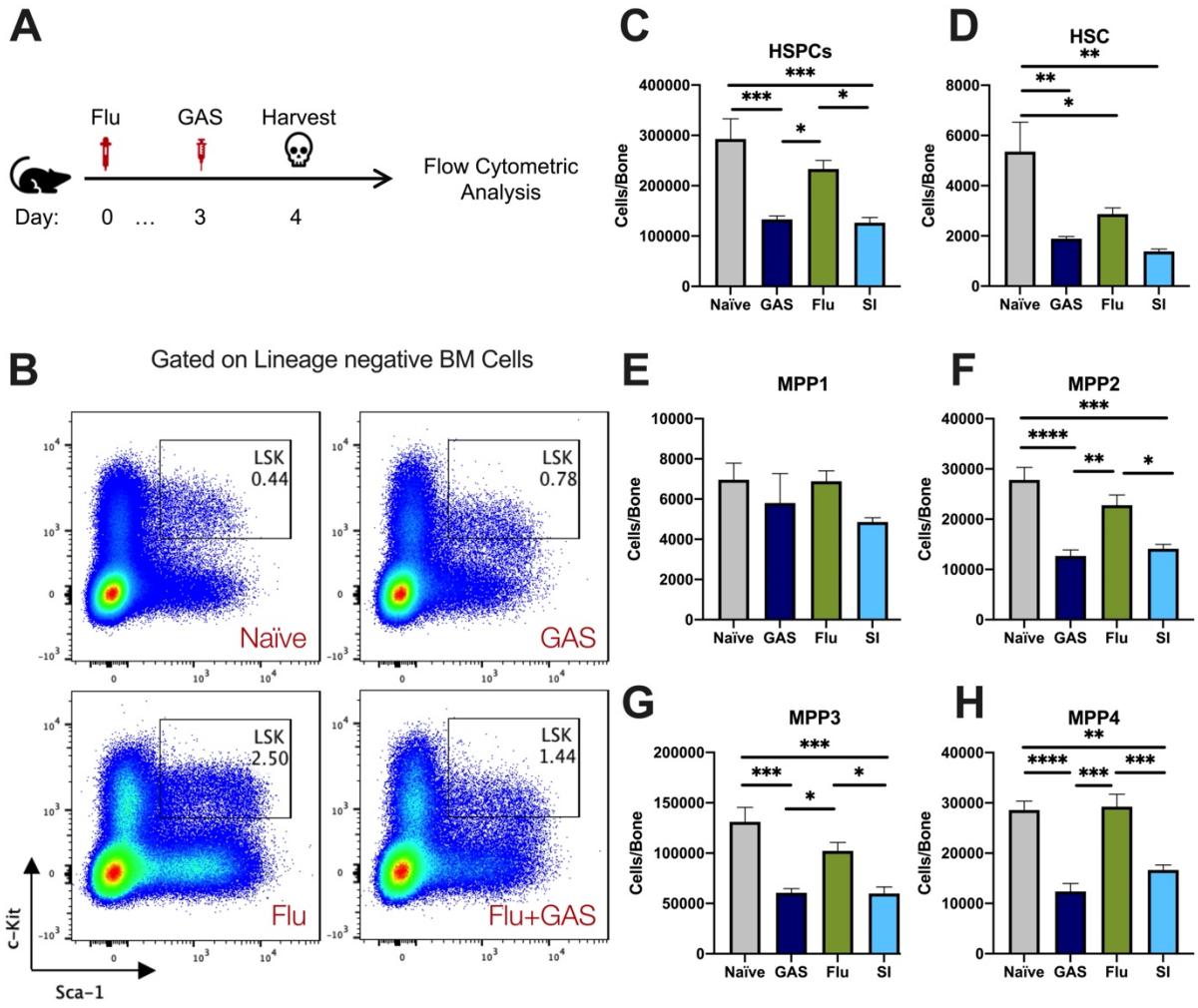

Supplemental figure 1. Superinfection further depletes HSPCs and HSCs in the BM. (A) Experimental design of superinfection. (B) Flow cytometry plots of HSPCs (LSK) and their phenotypic expression of surface c-Kit and Sca-1. (C-H) Absolute number of HSPC, HSCs, and MPP subpopulations in the BM of naïve, GAS-infected, flu-infected, or superinfected mice. Data is representative of 3 independent experiments; n=5 mice/group. Comparison was done using One-Way ANOVA and Tukey's correction for multiple comparisons; *p<0.05, **p<0.01, ***p<0.001, ****p<0.0001.

Supplemental figure 2

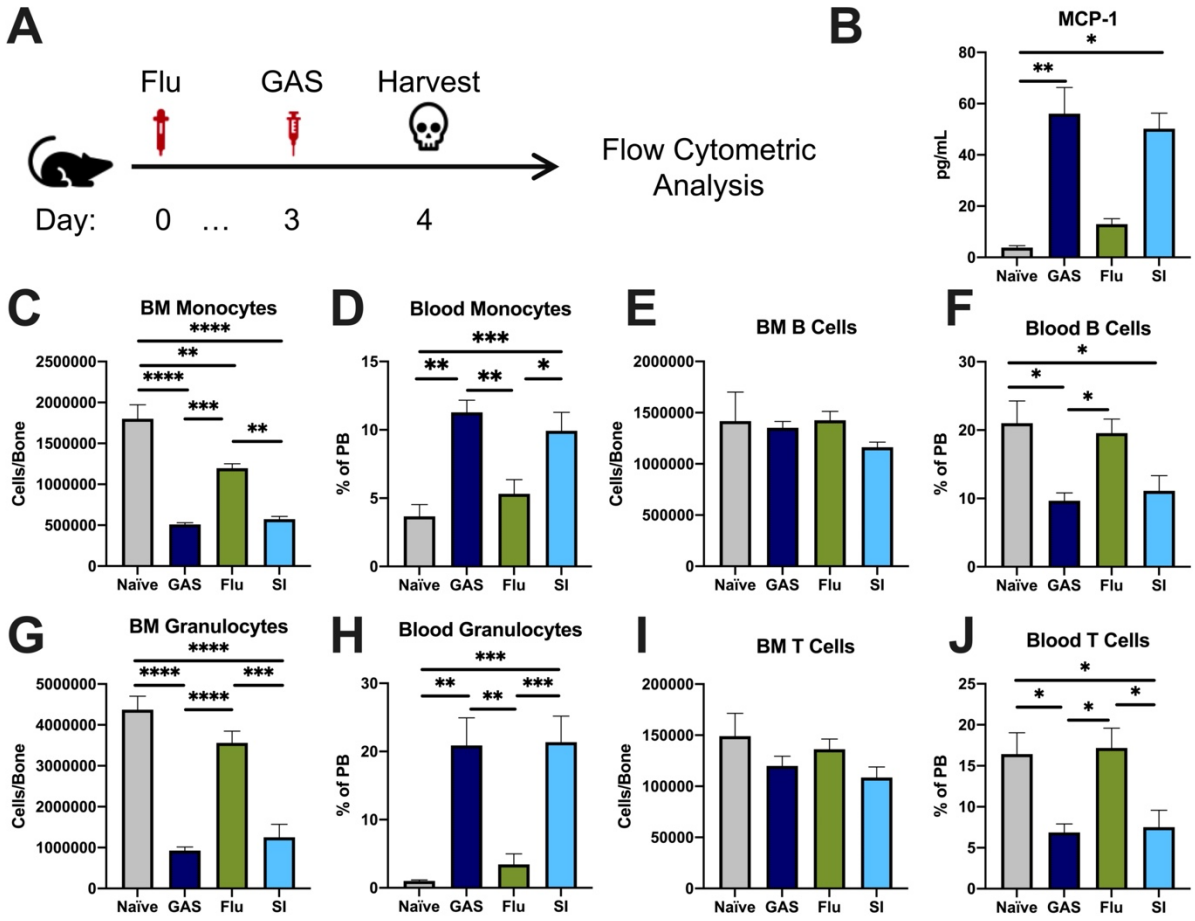

Supplemental Figure 2. GAS infection and superinfection promotes exit of myeloid cells from BM into circulation. (A) Experimental time frame of superinfection and BM analysis. (B) Serum levels of MCP-1 of naïve and mice infected with GAS, flu, or both pathogens. Absolute number of (C) monocytes, (E) B cells, (G) granulocytes, and (I) T cells in the BM of naïve and infected mice. Relative abundance of blood (D) monocytes, (F) B cells, (H) granulocytes, and (J) T cells. (B-J) Data is representative of 3 independent experiments; n = 3-5; Statistical comparison done using Unpaired t-test; *p<0.05, **p<0.01,***p<0.001, ****p<0.0001.

Supplemental figure 3

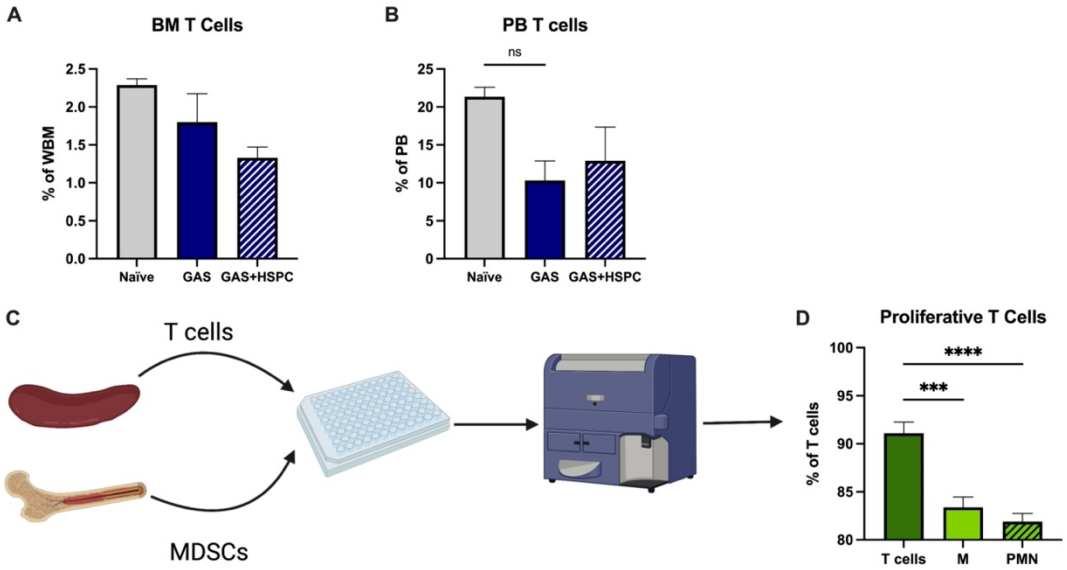

Supplemental Figure 3. MDSCs reduce activated T cell proliferation. Abundance of T cells in the(A) BM and (B) PB of mice; n=5-7 mice per group. (C) Experimental design of T cell suppression assay. Created with BioRender.com (D) Flow cytometric measurement of T cell proliferation by dilution of CellTrace Violet dye. 'M' represents M-MDSCs and 'PMN' represents PMN-MDSCs. Data is representative of at least 2 experiments. Statistical comparison done using One Way ANOVA and Tukey's Correction for multiple comparisons; ***p<0.001, ****p<0.0001.

Tables

Population	Markers
HSC	Lin- ckit+ CD150+ CD48- CD34- Flk2-
CD41+ HSCs	Lin- ckit+ CD150+ CD48- CD34- Flk2- CD41+
Donor HSPCs	Lin- ckit+ Sca1+
HSPCs	Lin- ckit+
MPP1	Lin- ckit+ CD150+ CD48- CD34+ Flk2-
MPP2	Lin- ckit+ CD150+ CD48+ Flk2-
MPP3	Lin- ckit+ CD150- CD48+ CD34+ Flk2-
MPP4	Lin- ckit+ CD150- CD48+ CD34+ Flk2+
GMP	Lin- ckit+ CD41- CD150- CD16/32+
MkP	Lin- ckit+ CD150+ CD41+
Myeloid cells	Gr1+ Mac1+ B220- CD4- CD8-
B cells	Gr1- Mac1- B220+ CD4- CD8-
T Cells	Gr1- Mac1- B220- CD4+ CD8- or Gr1- Mac1- B220- CD4- CD8+
Granulocytes	Gr1+ Mac1+ B220- CD4- CD8- SSC-mid F4/80-
Eosinophils	Gr1- Mac1+ B220- CD4- CD8- SSC^{Hi}
Macrophages	Gr1+ Mac1+ B220- CD4- CD8- SSC^{low} F4/80+
Monocytes	Mac1+ B220- CD4- CD8- SSC^{low}
PMN-MDSC	CD11b+ Ly6G+ $Ly6C^{low}$CD244+
M-MDSC	CD11b+ Ly6G- $Ly6C^{hi}$

Table 1: Surface markers for flow cytometry. Hematopoietic cell populations identified by flow cytometry were characterized using the listed surface markers. Lineage (Lin) markers include Gr1, CD11b, B220, CD4, CD8, and Ter119.

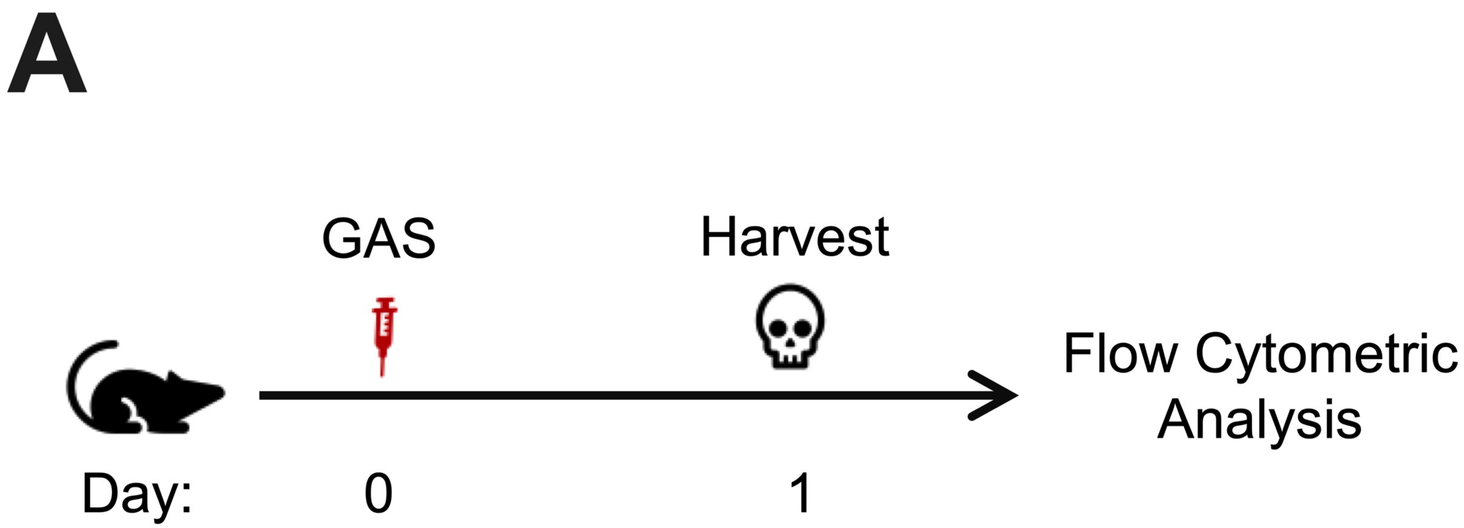

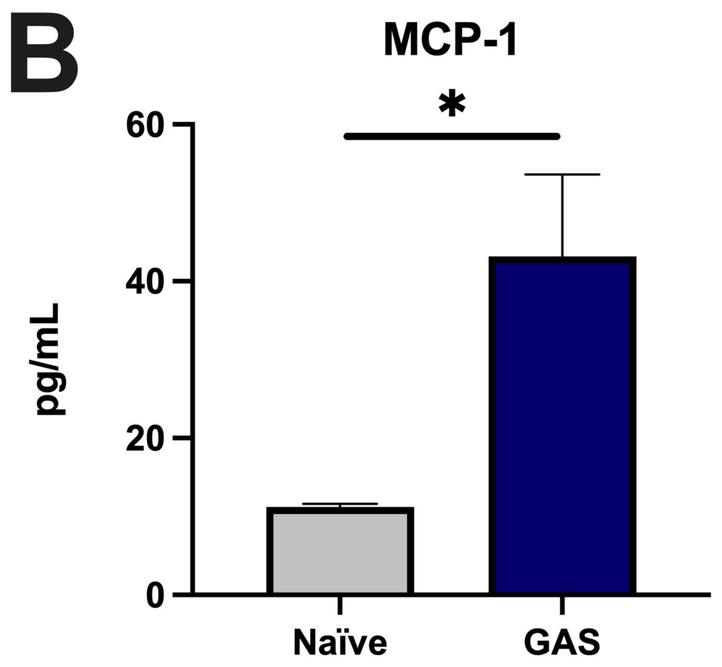

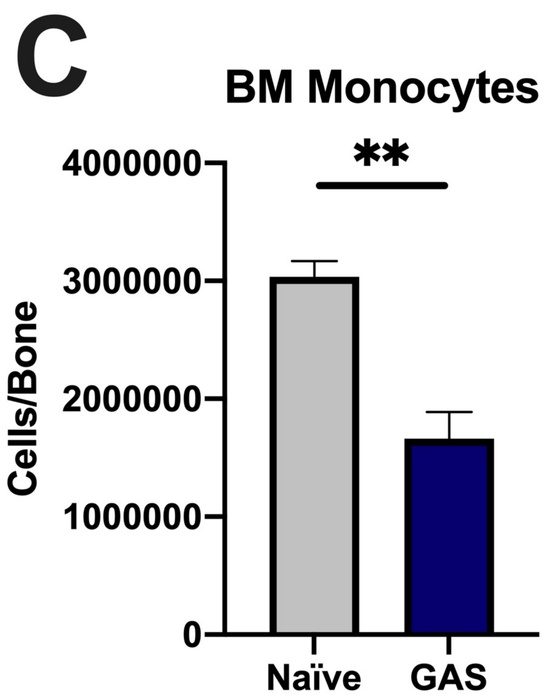

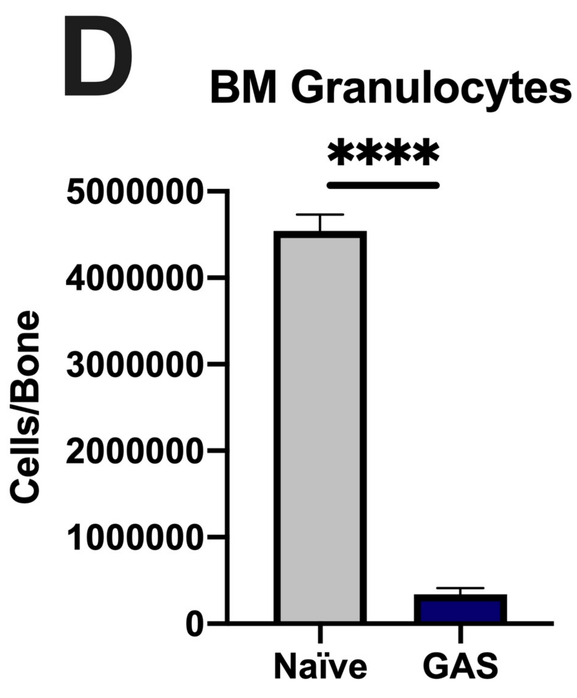

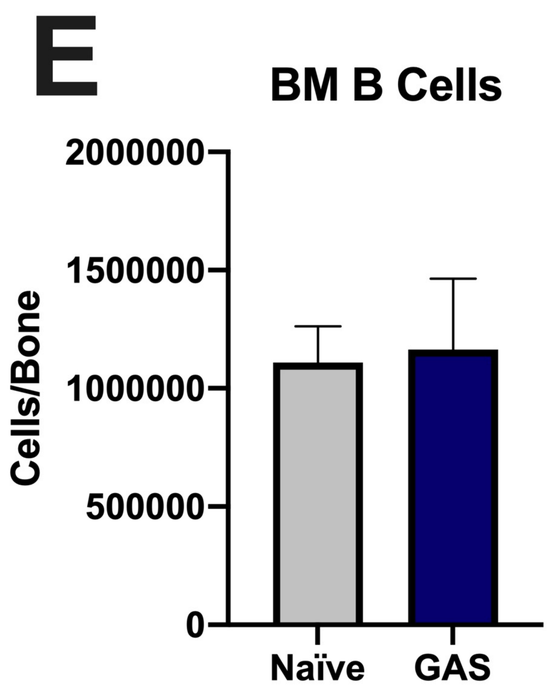

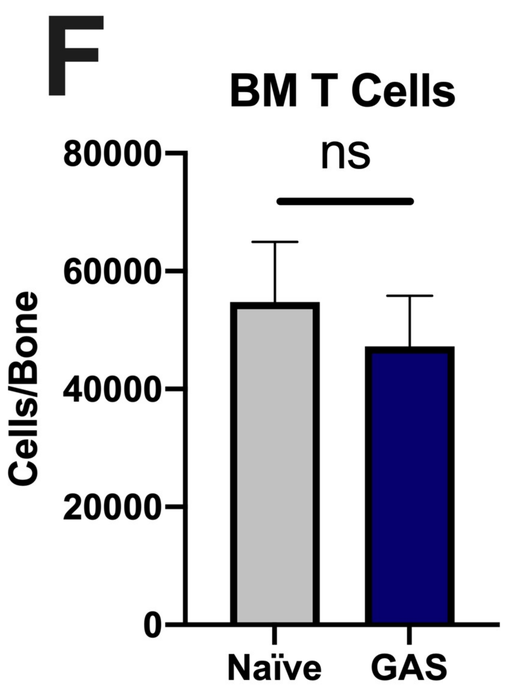

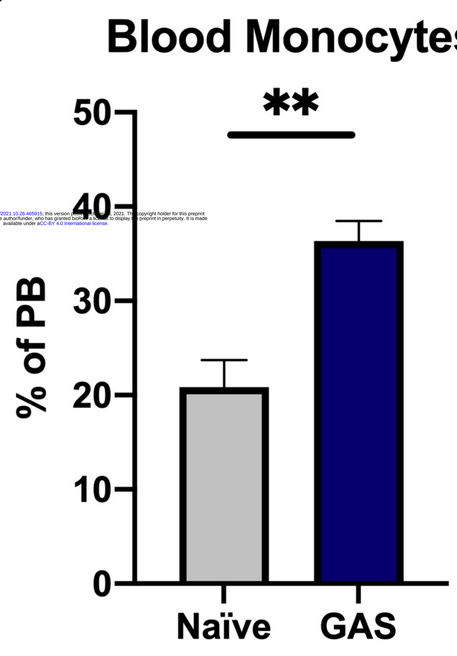

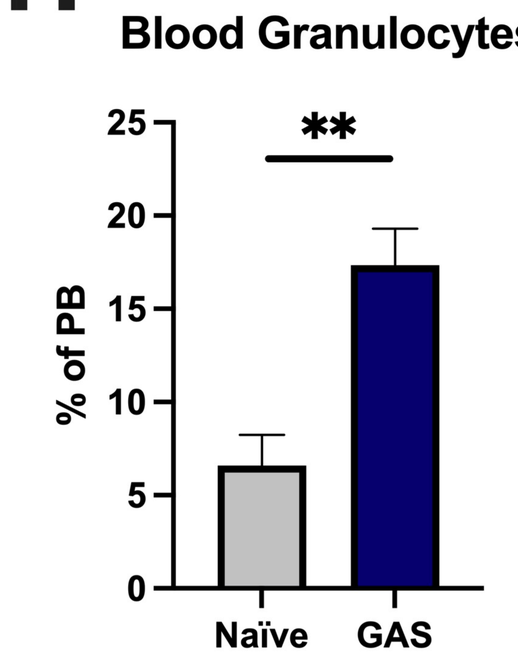

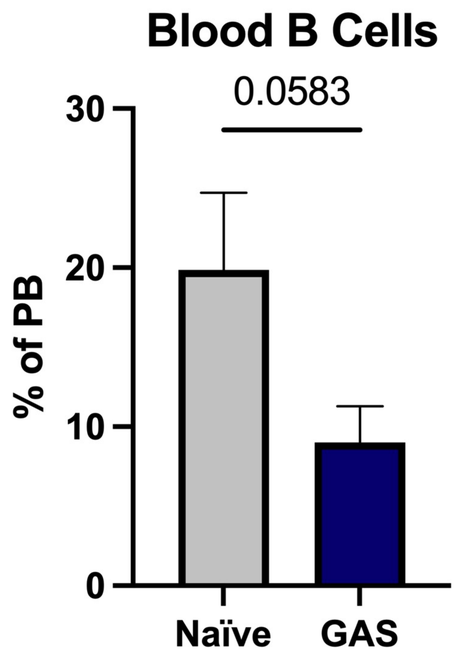

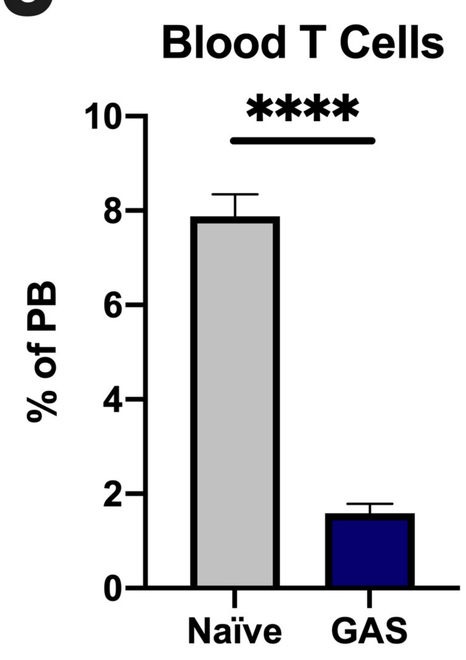

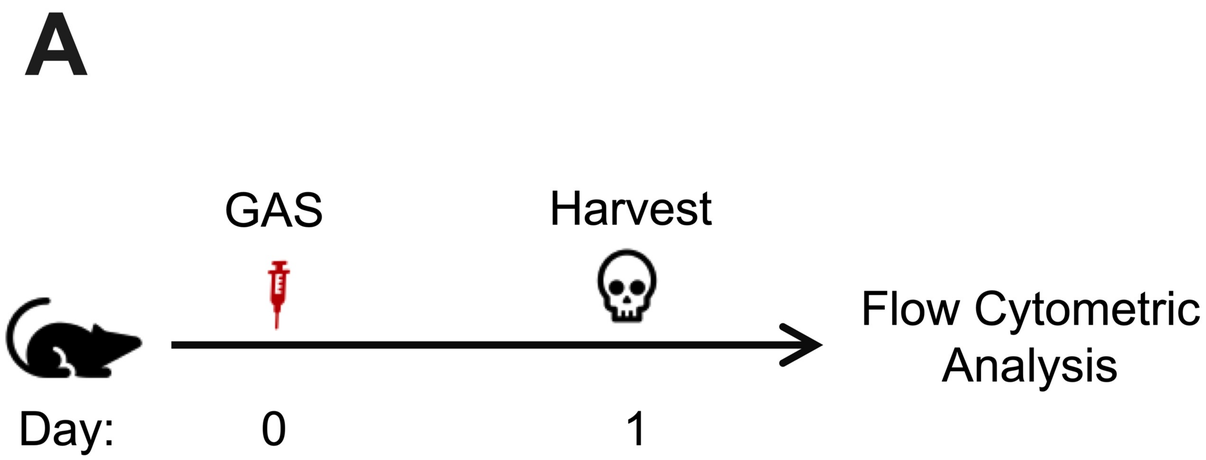
A
GAS
Harvest
Flow Cytometric Analysis
Day:
0
1

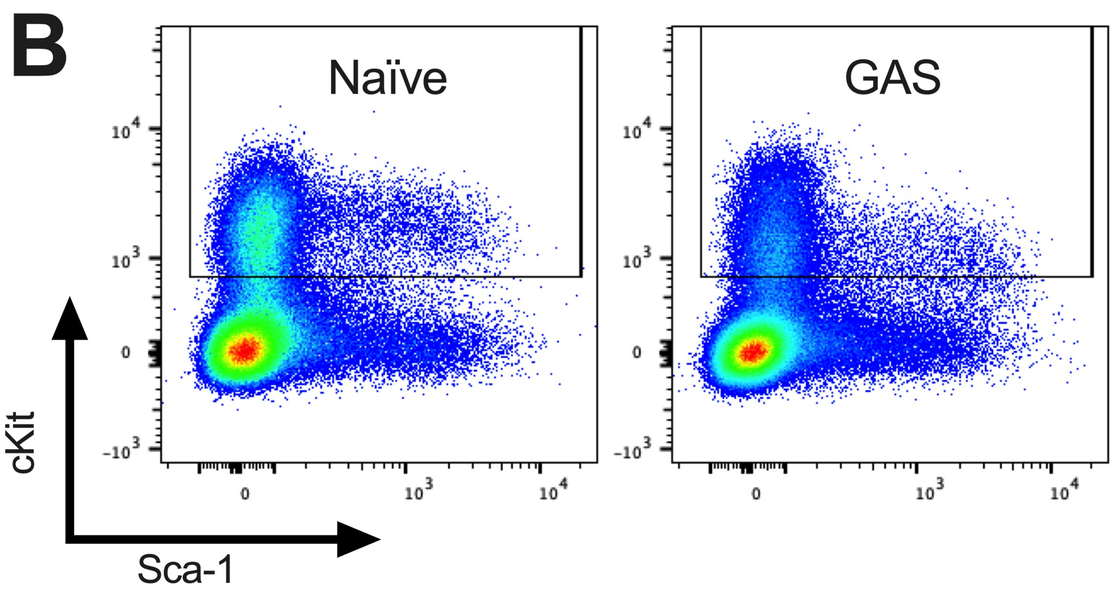
B
Naïve
GAS
cKit
Sca-1

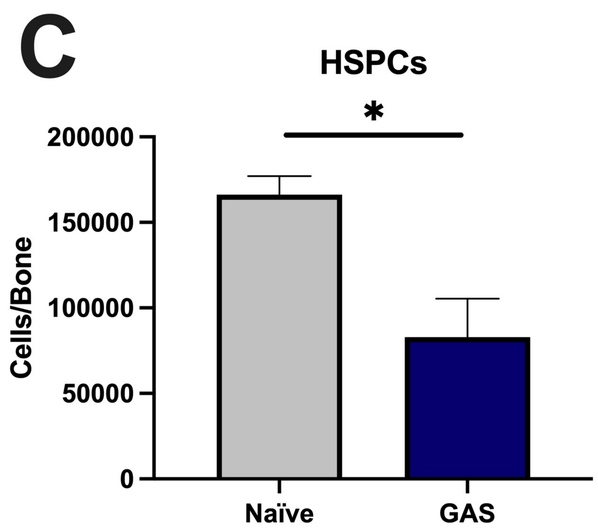
C
HSPCs
*
Cells/Bone
Naïve
GAS

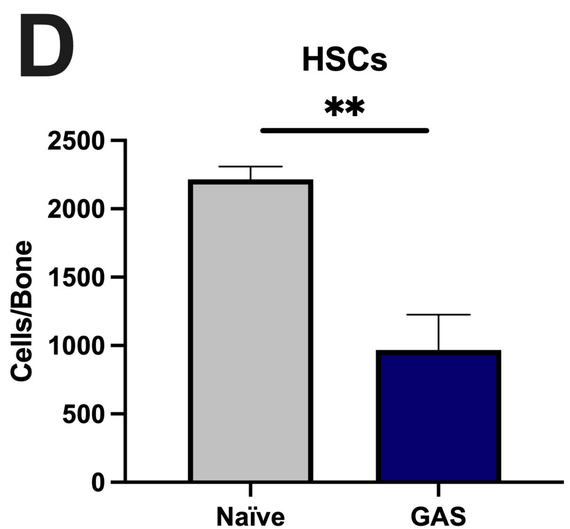
D
HSCs
**
Cells/Bone
Naïve
GAS

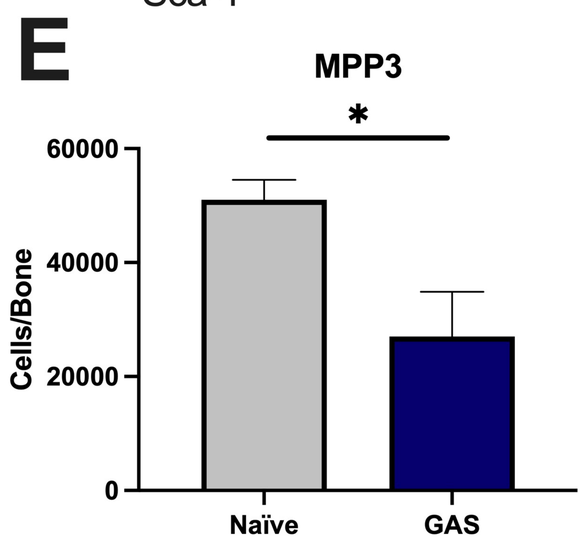
E
MPP3
*
Cells/Bone
Naïve
GAS

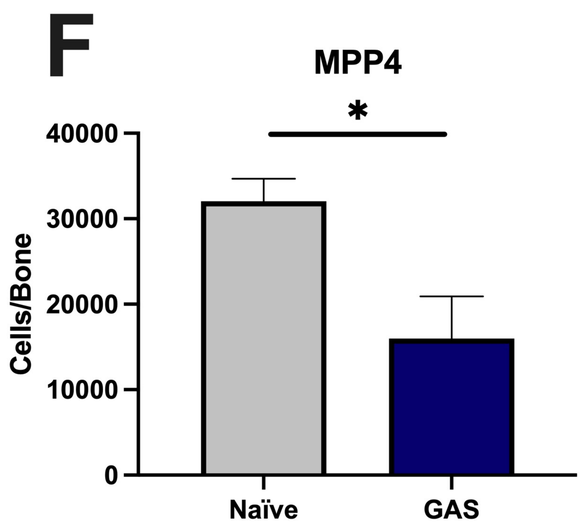
F
MPP4
*
Cells/Bone
Naïve
GAS

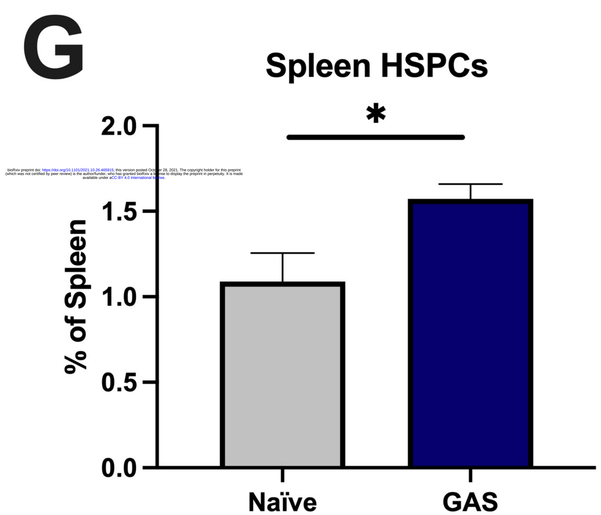
G
Spleen HSPCs
*
% of Spleen
Naïve
GAS

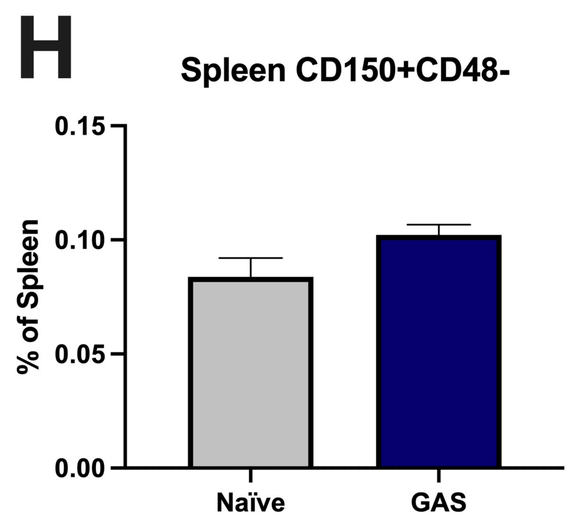
H
Spleen CD150+CD48-
% of Spleen
Naïve
GAS

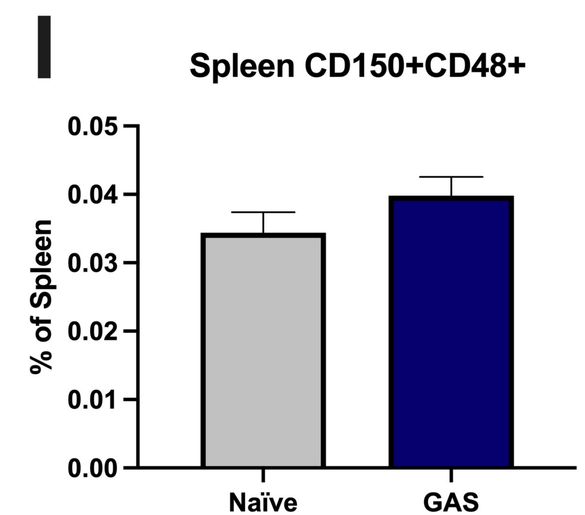
I
Spleen CD150+CD48+
% of Spleen
Naïve
GAS

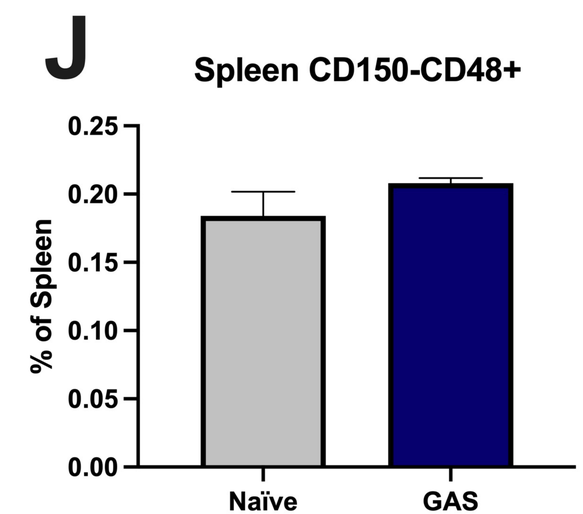
J
Spleen CD150-CD48+
% of Spleen
Naïve
GAS

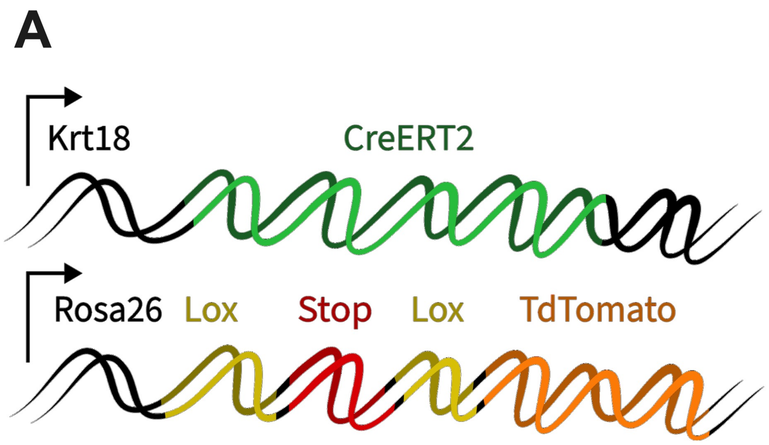
A
Krt18
CreERT2
Rosa26
Lox
Stop
Lox
TdTomato

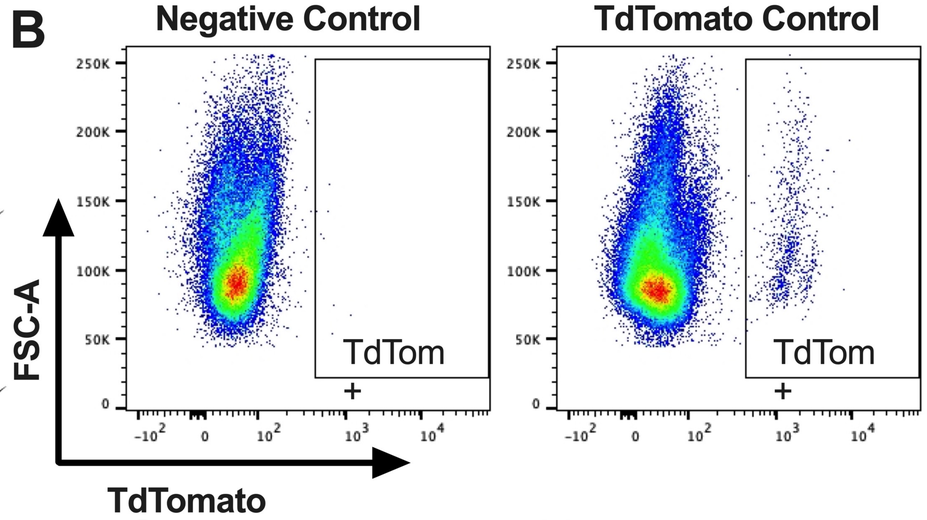
B
Negative Control
TdTomato Control
FSC-A
TdTomato
TdTom
+

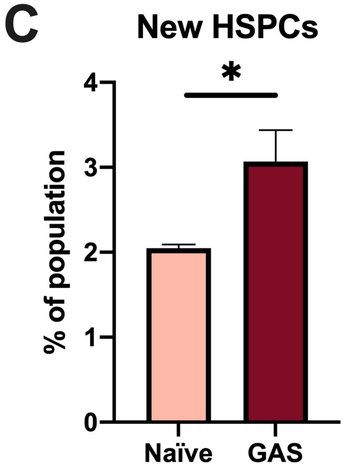
C
New HSPCs
% of population
Naïve
GAS
*

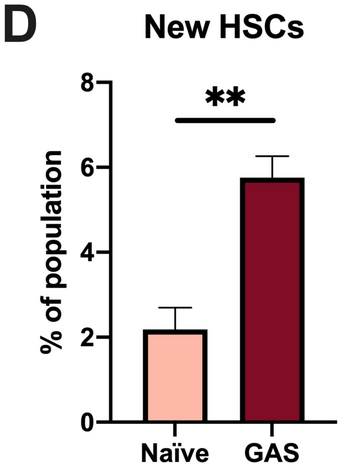
D
New HSCs
% of population
Naïve
GAS
**

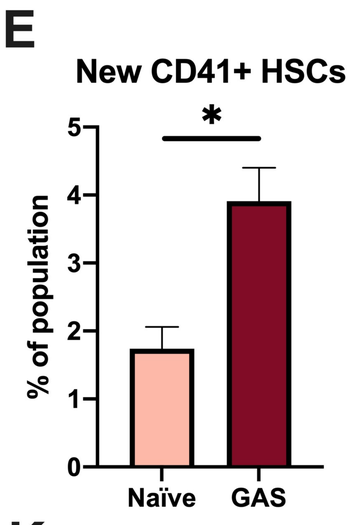
E
New CD41+ HSCs
% of population
Naïve
GAS
*

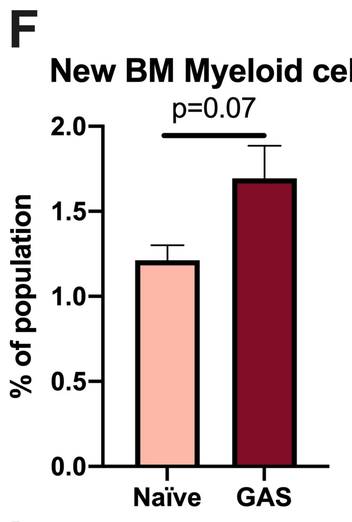
F
New BM Myeloid cells
p=0.07
% of population
Naïve
GAS

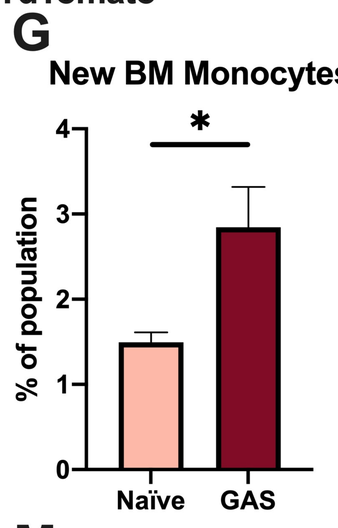
G
New BM Monocytes
% of population
Naïve
GAS
*

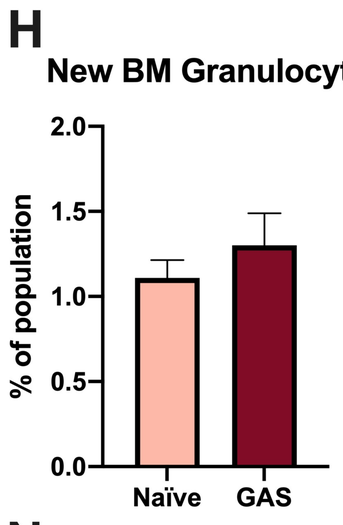
H
New BM Granulocytes
% of population
Naïve
GAS

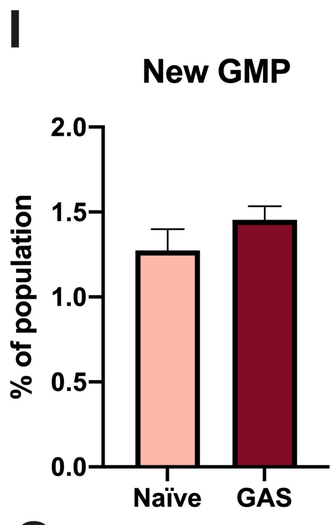
I
New GMP
% of population
Naïve
GAS

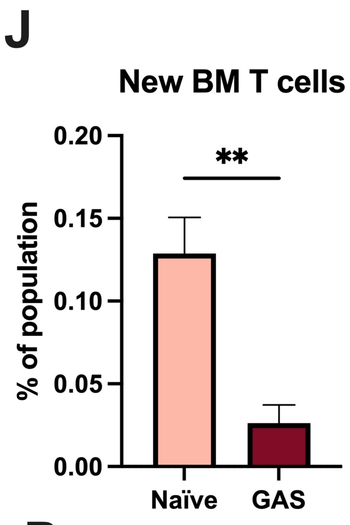
J
New BM T cells
% of population
Naïve
GAS
**

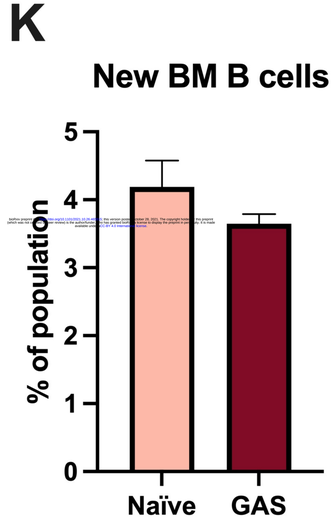
K
New BM B cells
% of population
Naïve
GAS

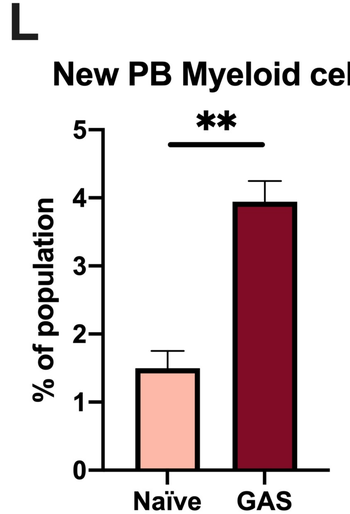
L
New PB Myeloid cells
% of population
Naïve
GAS
**

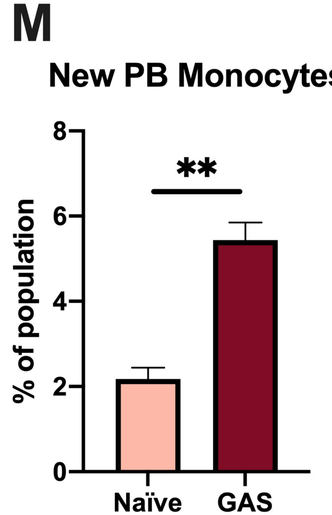
M
New PB Monocytes
% of population
Naïve
GAS
**

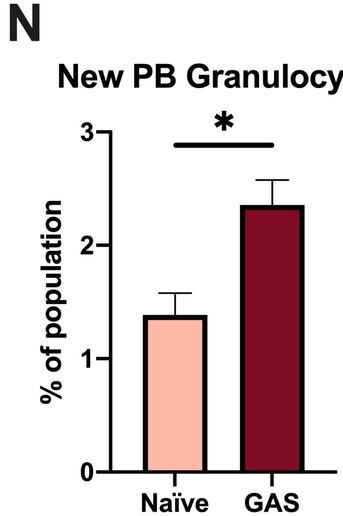
N
New PB Granulocytes
% of population
Naïve
GAS
*

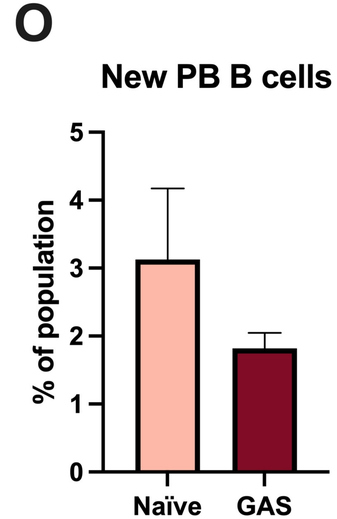
O
New PB B cells
% of population
Naïve
GAS

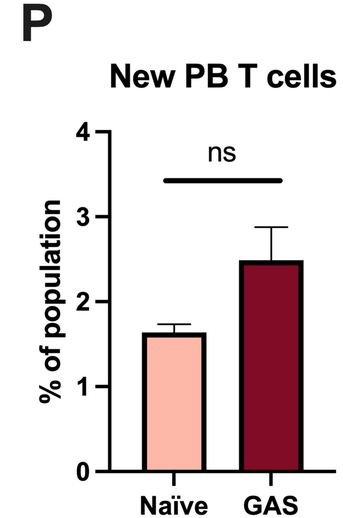
P
New PB T cells
% of population
Naïve
GAS
ns

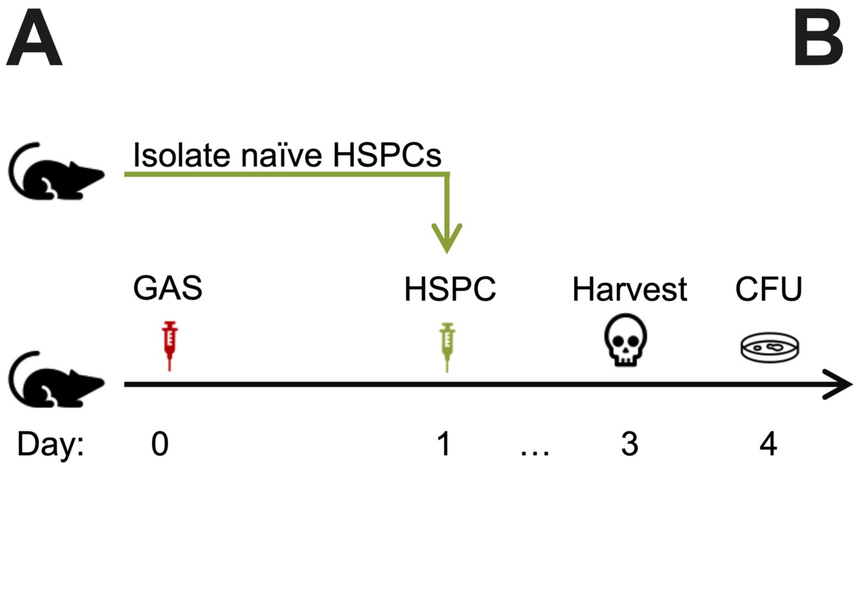
A
Isolate naïve HSPCs
GAS
HSPC
Harvest
CFU
Day:
0
1
…
3
4

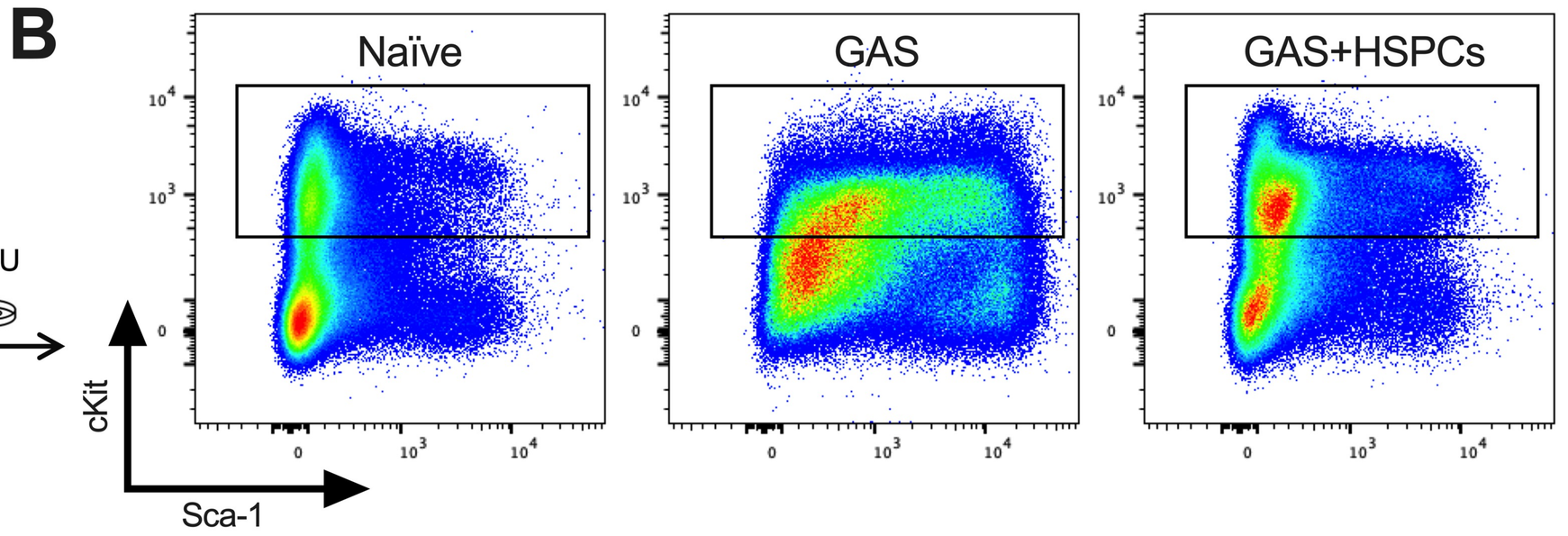
B
Naïve
GAS
GAS+HSPCs
cKit
Sca-1

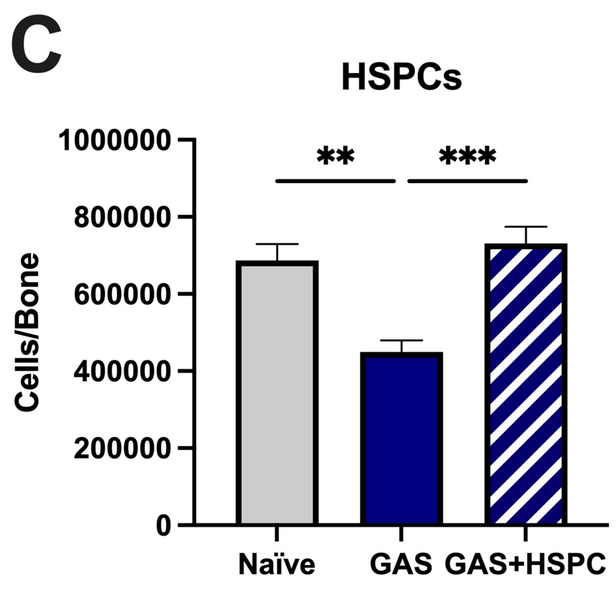
C
HSPCs
Cells/Bone
Naïve
GAS
GAS+HSPC

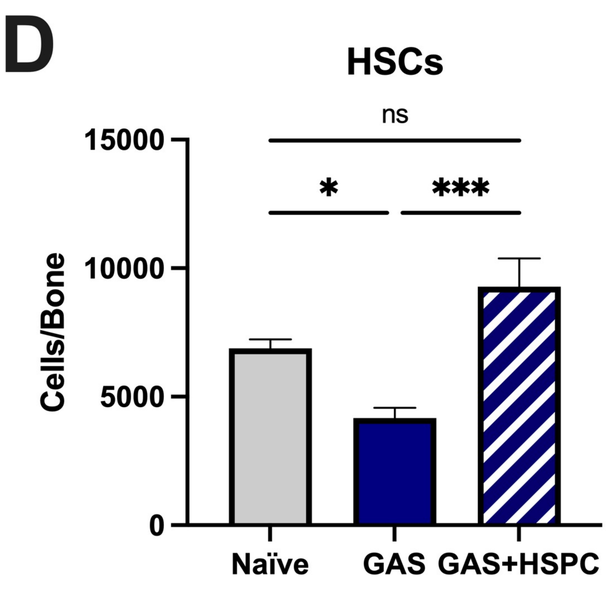
D
HSCs
ns
Cells/Bone
Naïve
GAS
GAS+HSPC

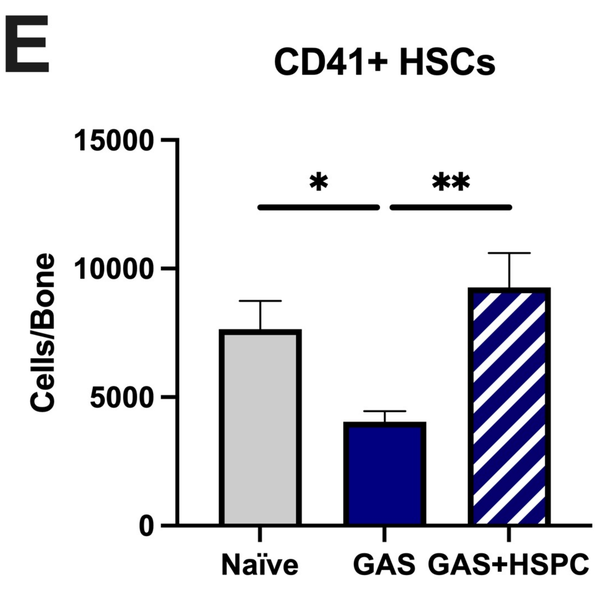
E
CD41+ HSCs
Cells/Bone
Naïve
GAS
GAS+HSPC

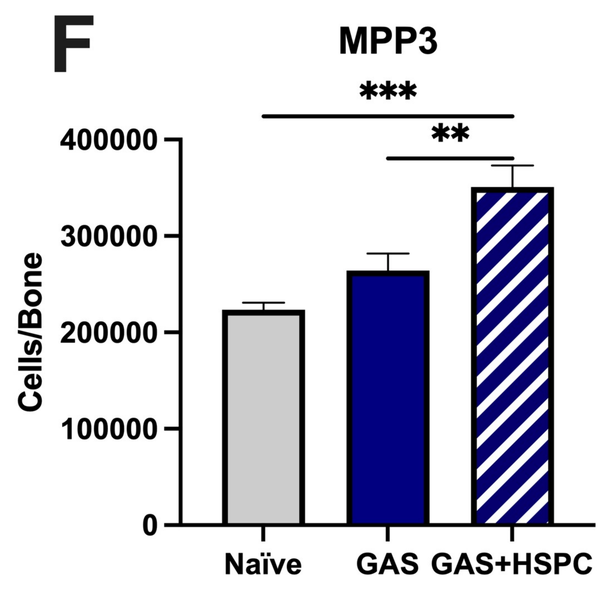
F
MPP3
Cells/Bone
Naïve
GAS
GAS+HSPC

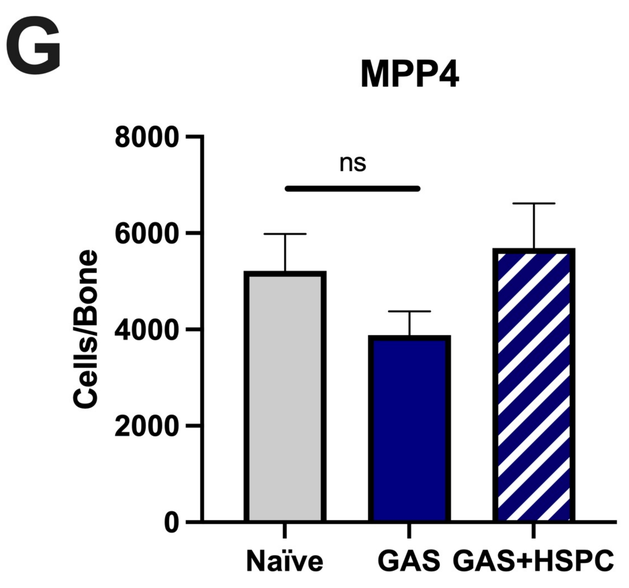
G
MPP4
ns
Cells/Bone
Naïve
GAS
GAS+HSPC

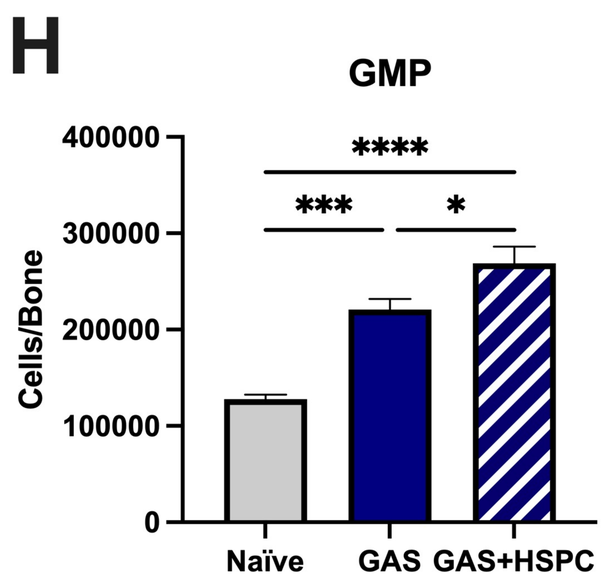
H
GMP
Cells/Bone
Naïve
GAS
GAS+HSPC

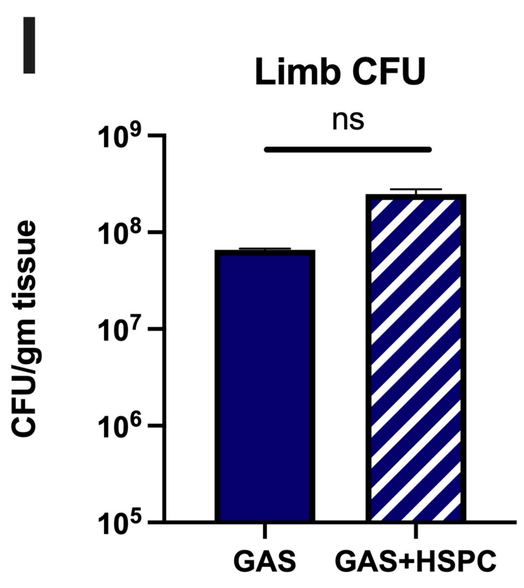
I
Limb CFU
ns
CFU/gm tissue
GAS
GAS+HSPC

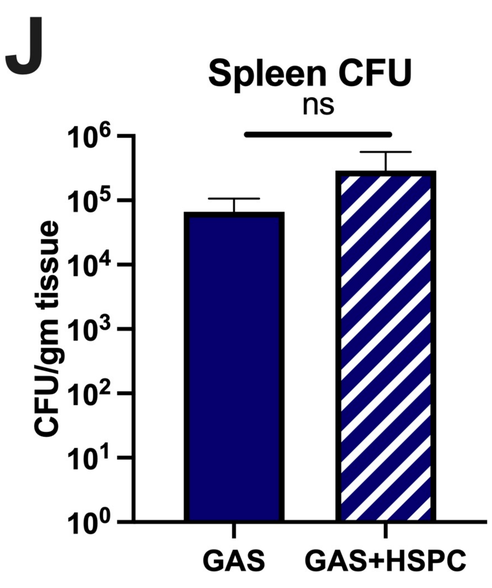
J
Spleen CFU
ns
CFU/gm tissue
GAS
GAS+HSPC

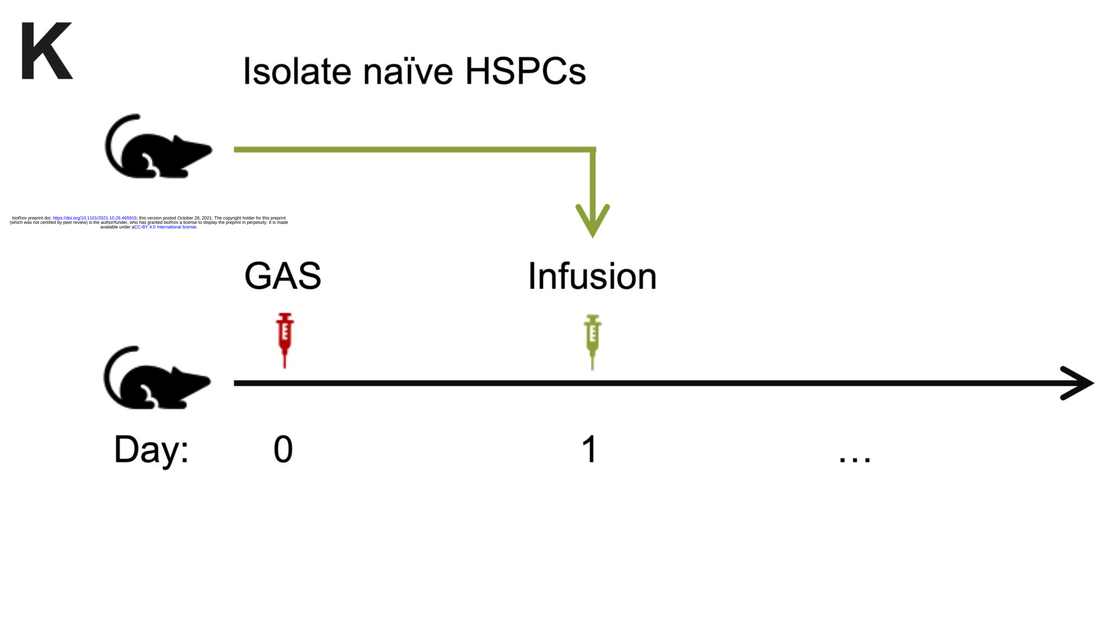
K
Isolate naïve HSPCs
GAS
Infusion
Day:
0
1
…

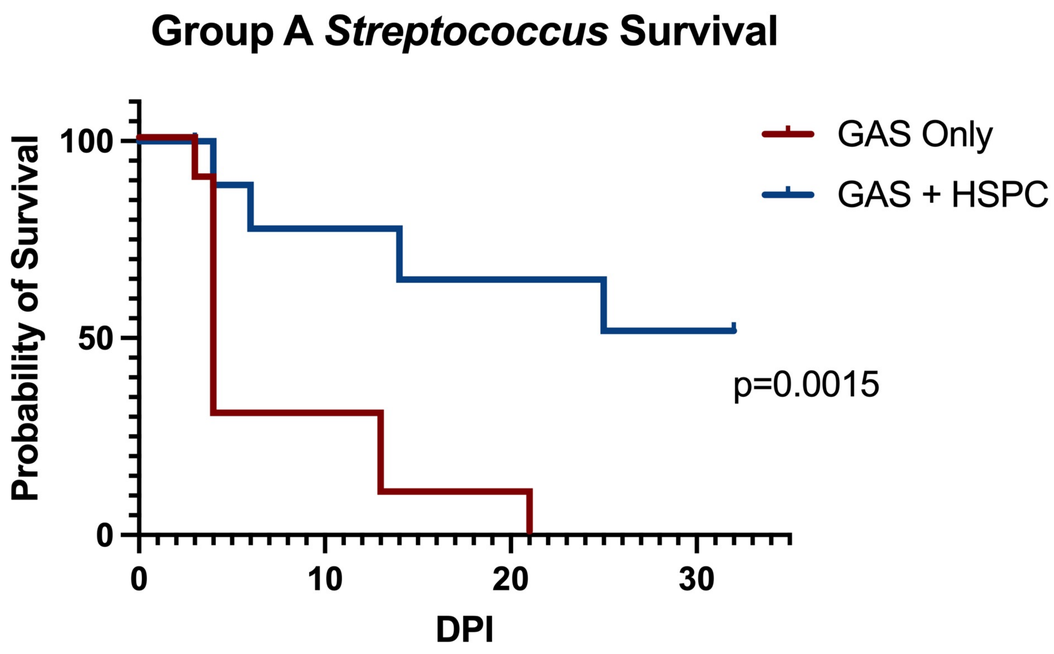
L
Group A Streptococcus Survival
Probability of Survival
DPI
GAS Only
GAS + HSPC
p=0.0015

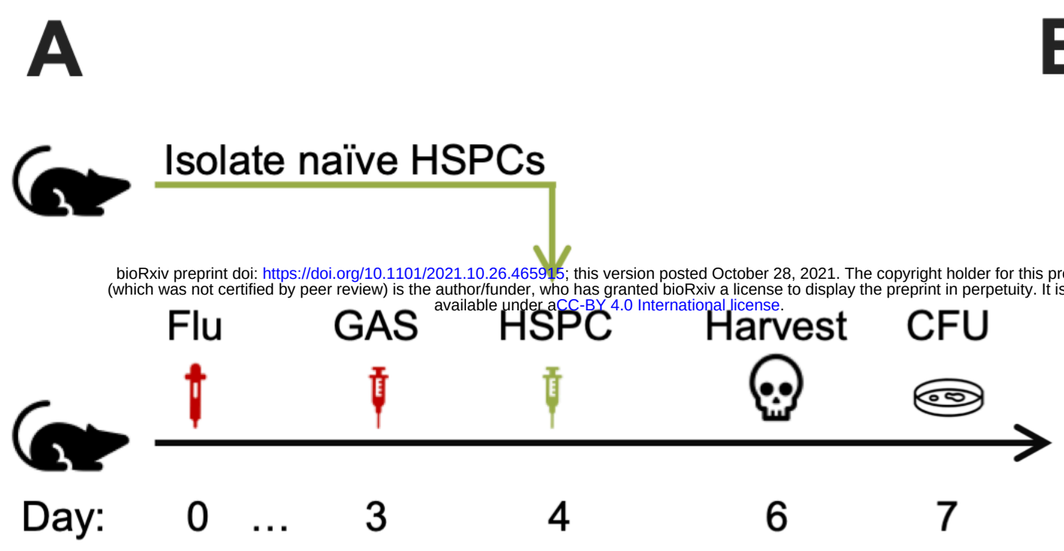

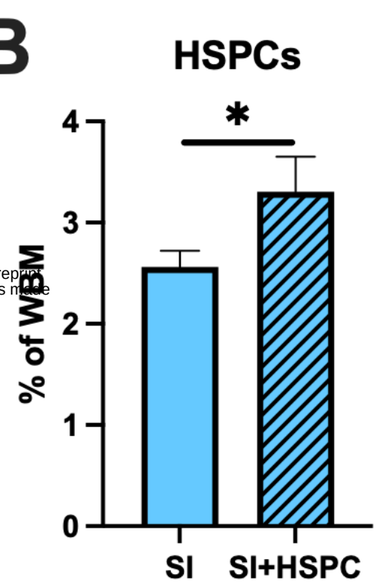

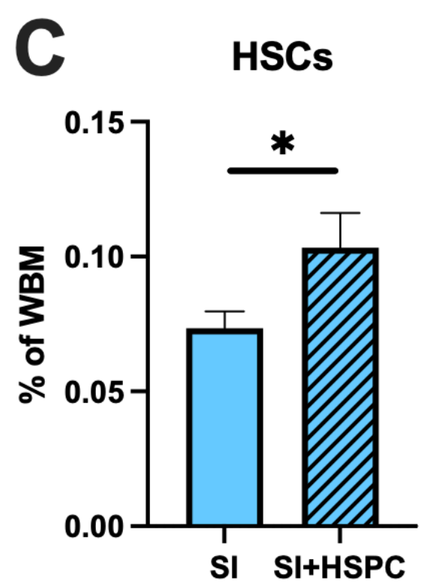

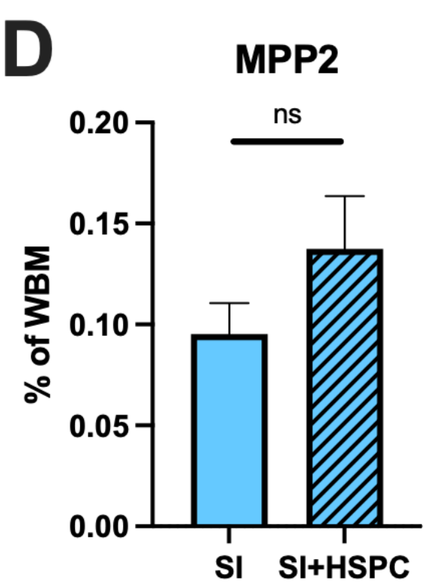

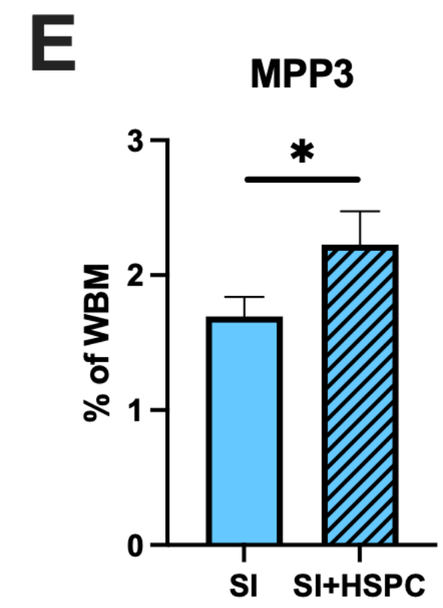

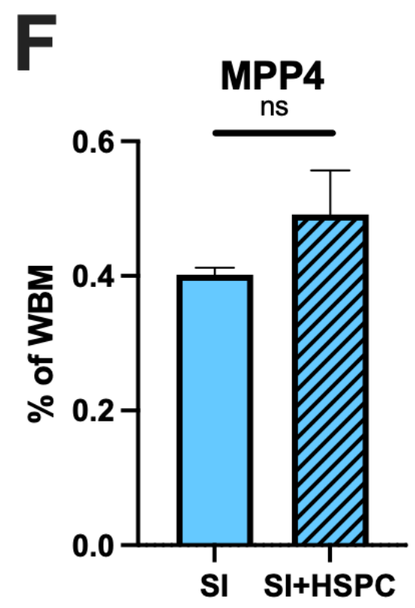

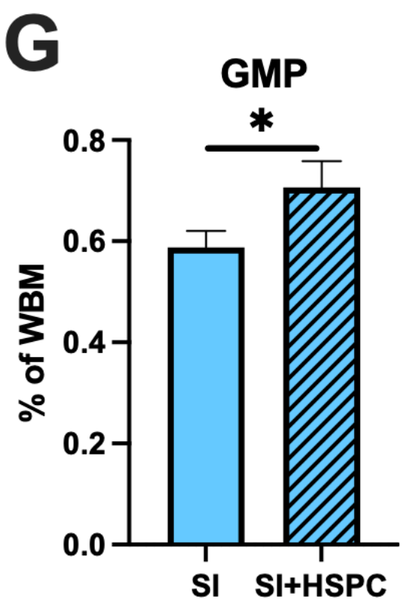

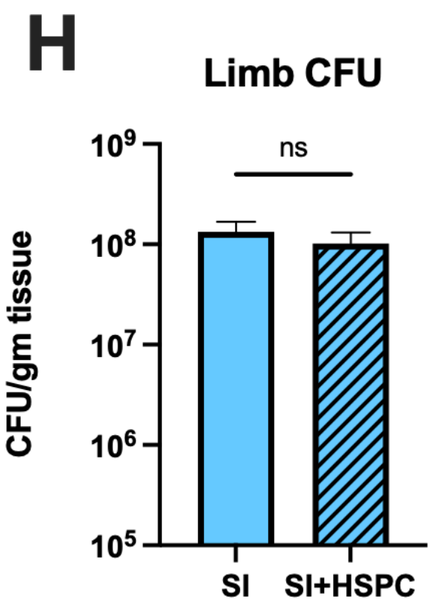

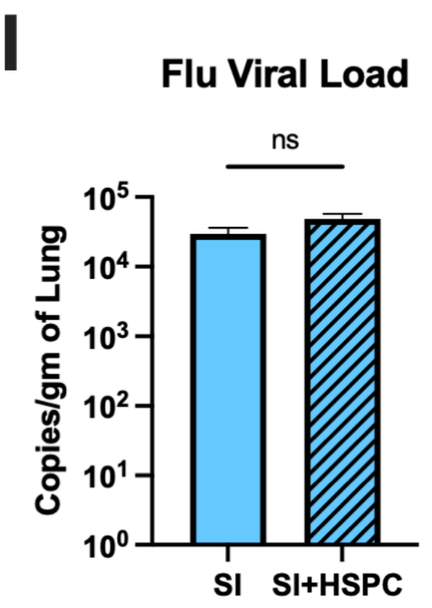

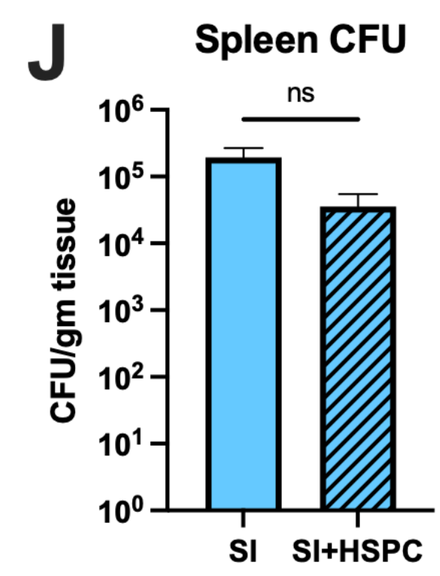

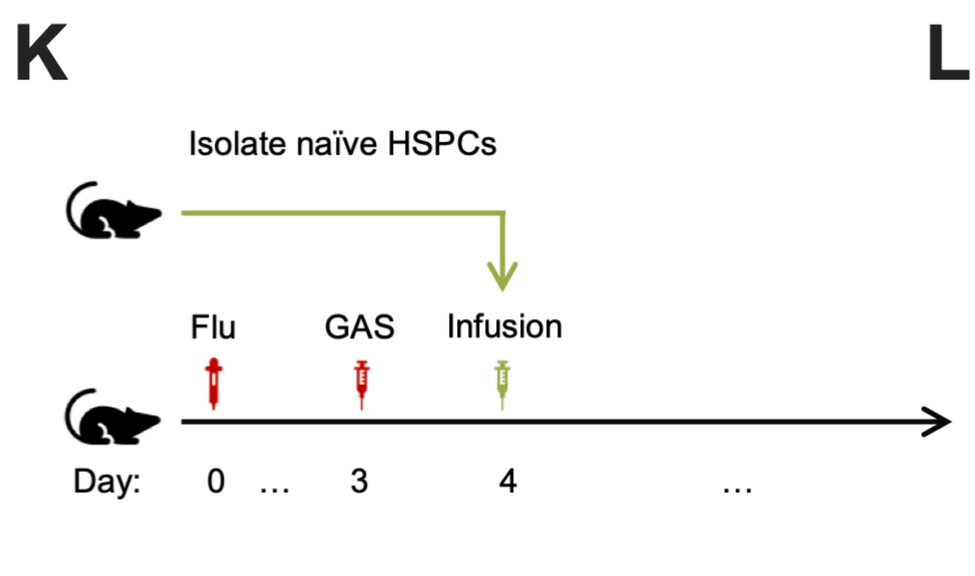

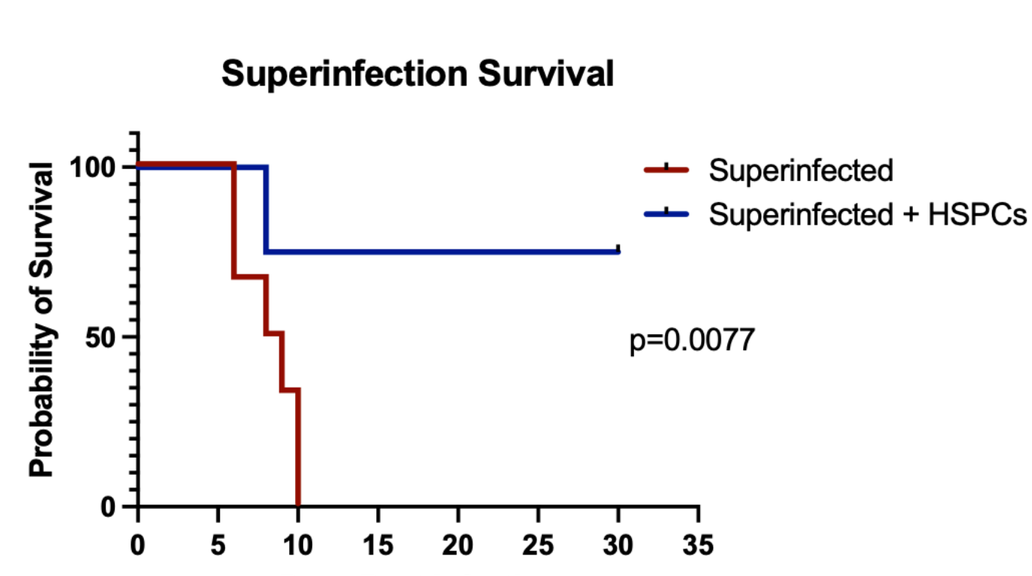

A Bone Marrow HSPCs

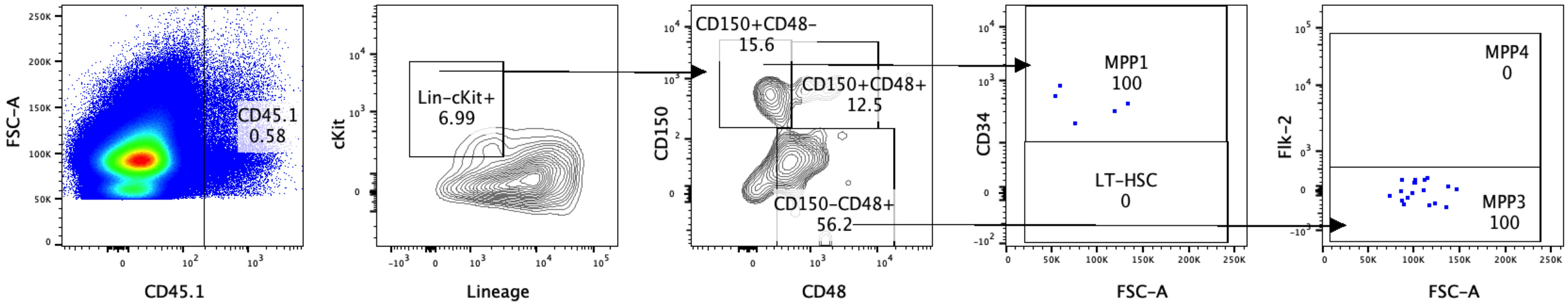

B Bone Marrow Lineage

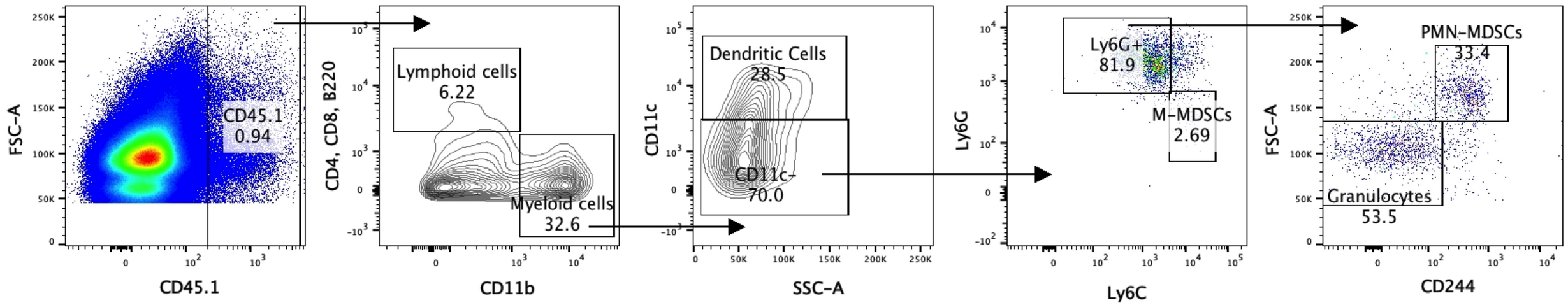

C Peripheral Blood Lineage

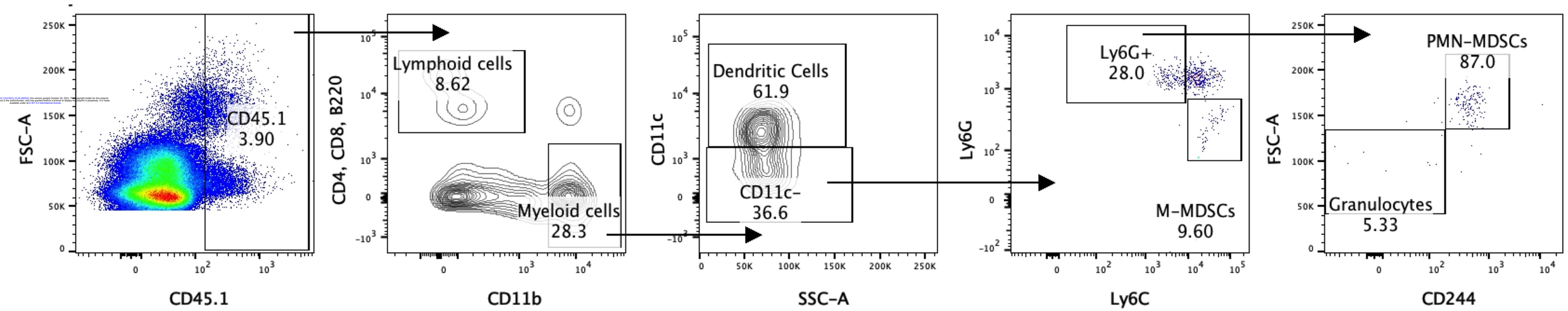

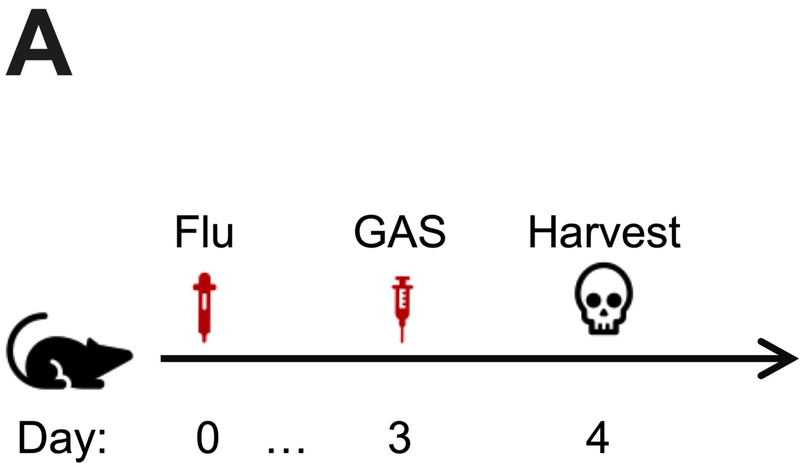
A
Flu
GAS
Harvest
Day:
0
…
3
4
Flow Cytometric Analysis

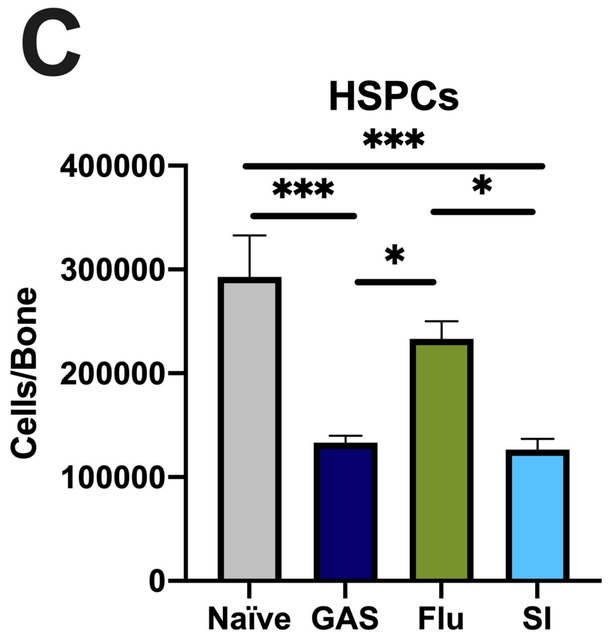
C
HSPCs
Cells/Bone
400000
300000
200000
100000
0
Naïve
GAS
Flu
SI

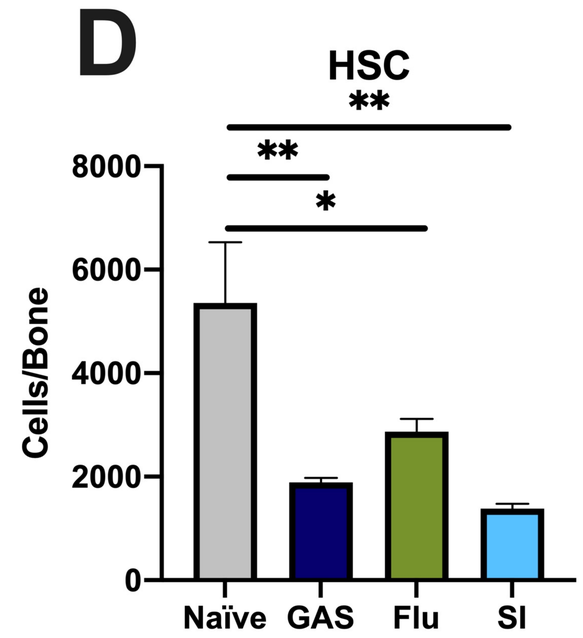
D
HSC
Cells/Bone
8000
6000
4000
2000
0
Naïve
GAS
Flu
SI

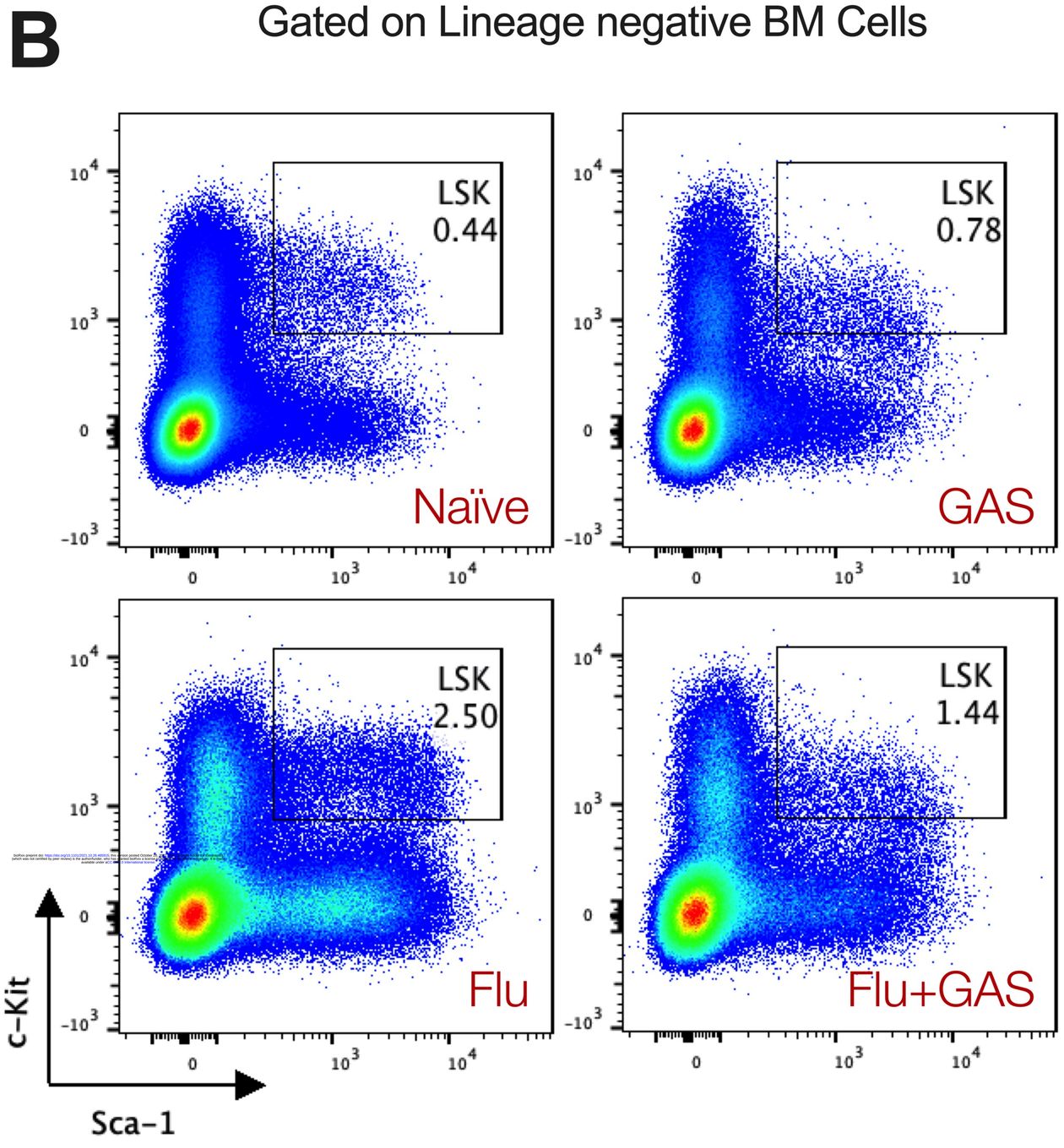
B
Gated on Lineage negative BM Cells
LSK
0.44
Naïve
LSK
0.78
GAS
LSK
2.50
Flu
LSK
1.44
Flu+GAS
c-Kit
Sca-1

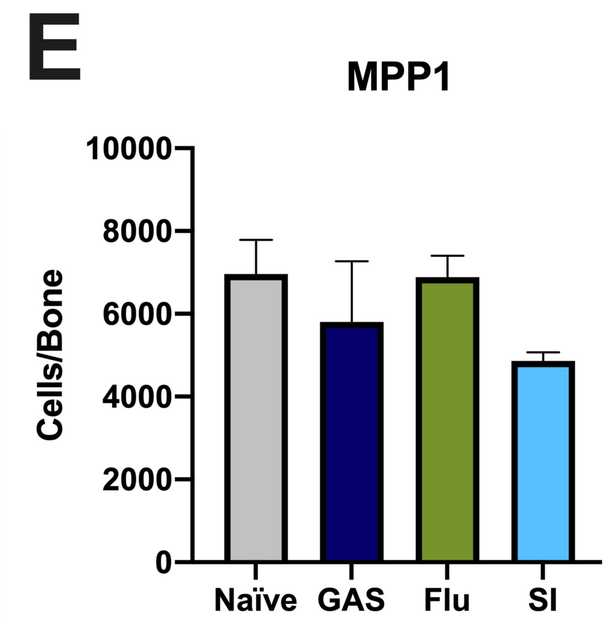
E
MPP1
Cells/Bone
10000
8000
6000
4000
2000
0
Naïve
GAS
Flu
SI

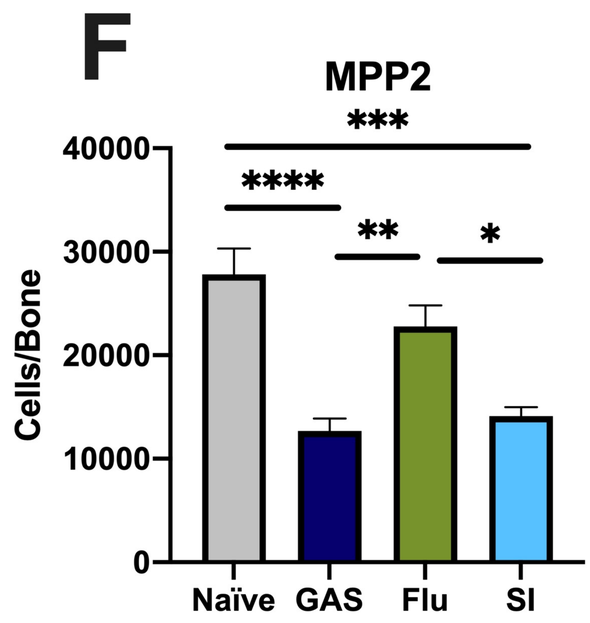
F
MPP2
Cells/Bone
40000
30000
20000
10000
0
Naïve
GAS
Flu
SI

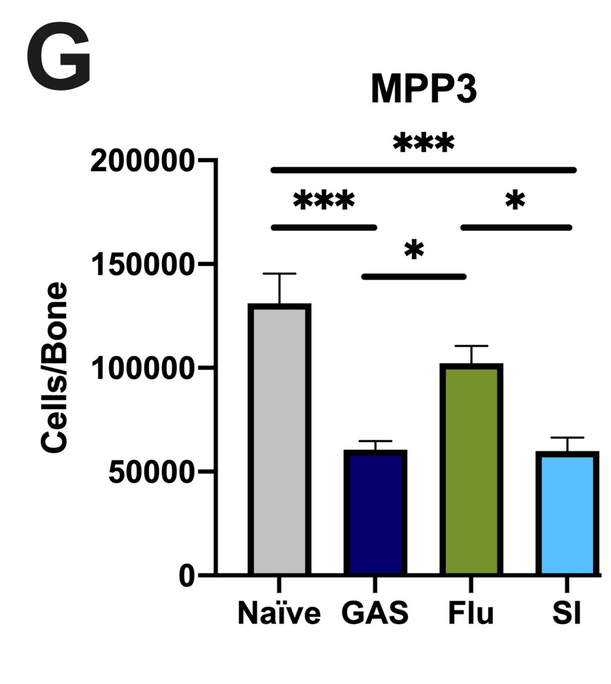
G
MPP3
Cells/Bone
200000
150000
100000
50000
0
Naïve
GAS
Flu
SI

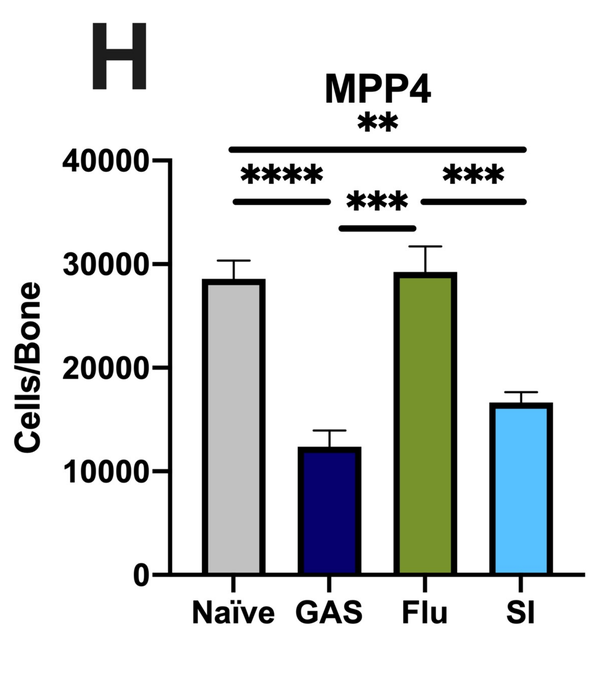
H
MPP4
Cells/Bone
40000
30000
20000
10000
0
Naïve
GAS
Flu
SI

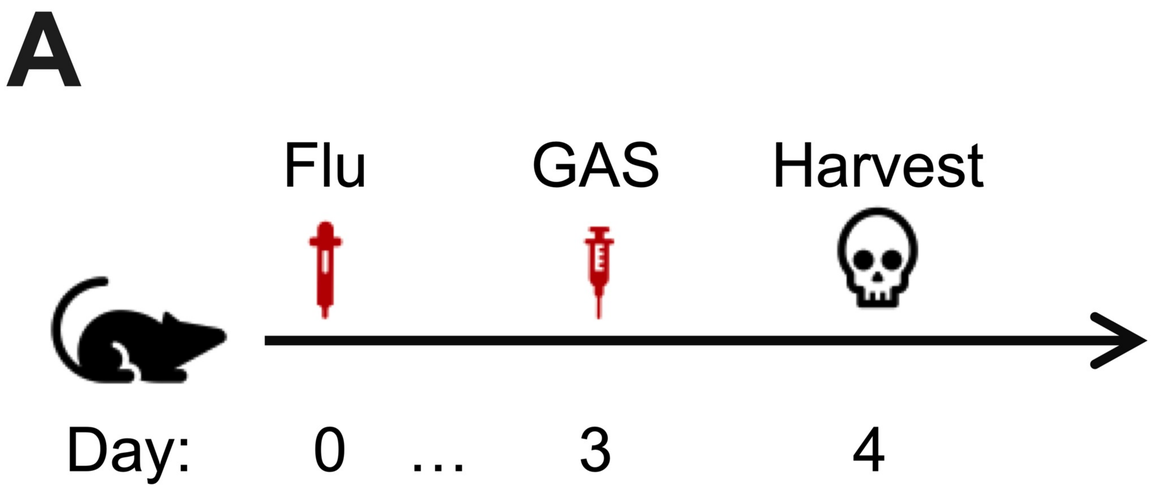

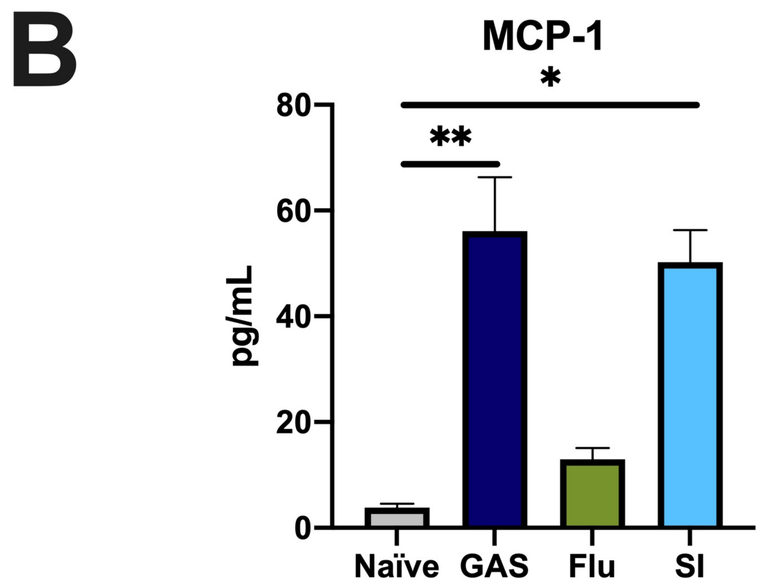

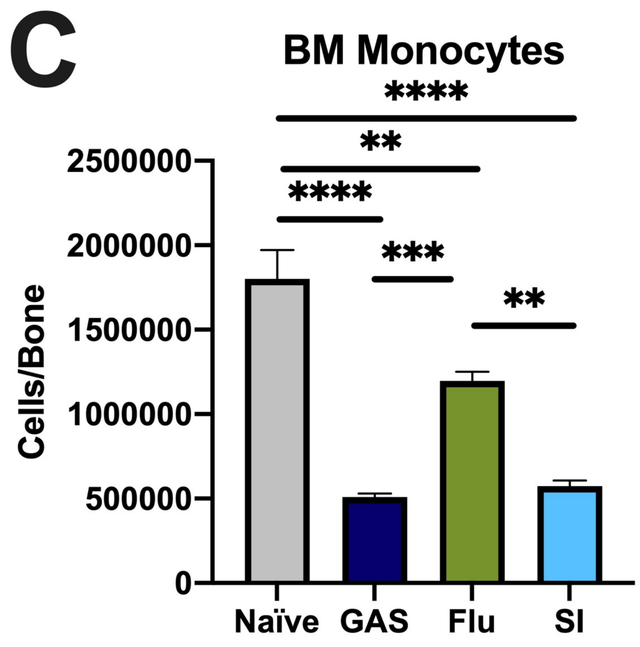

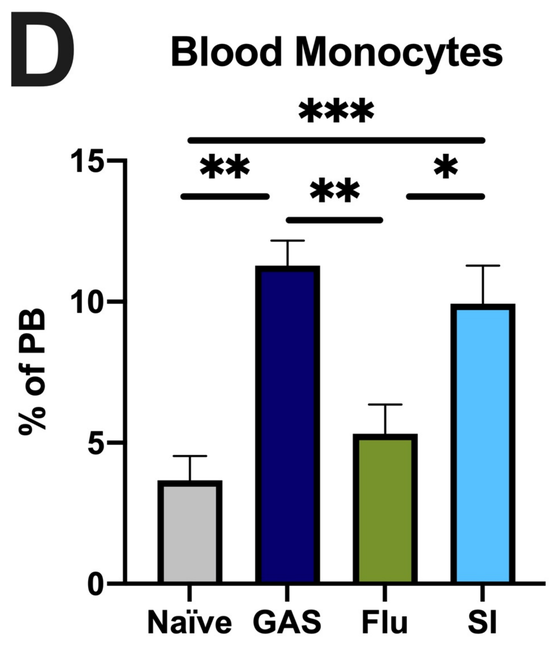

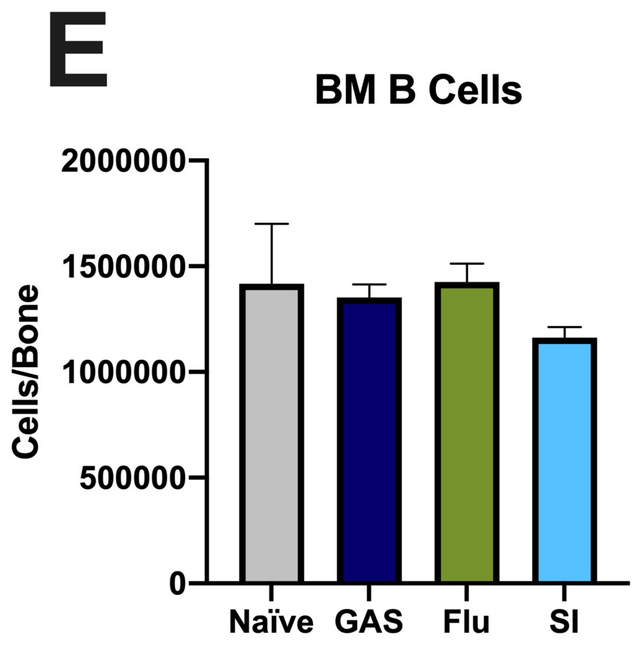

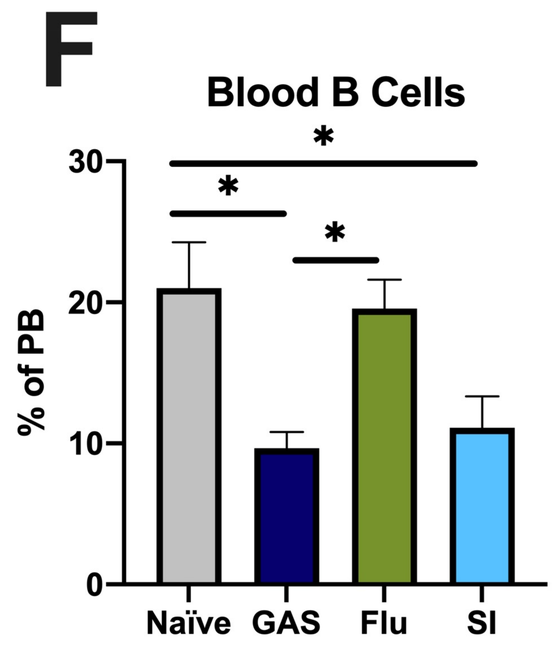

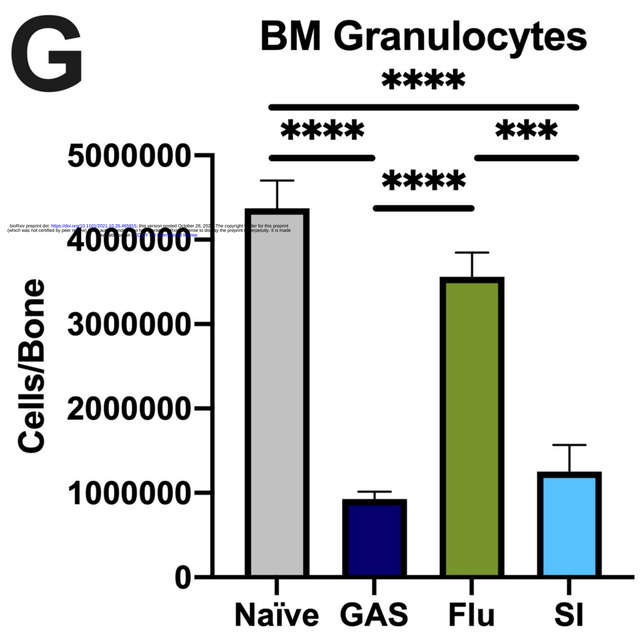

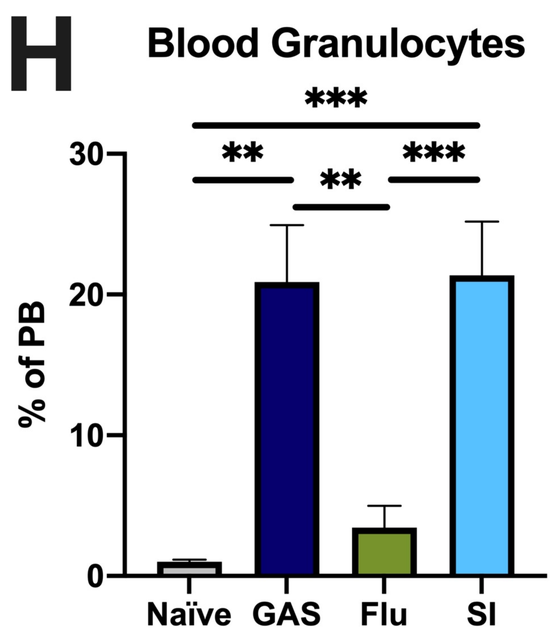

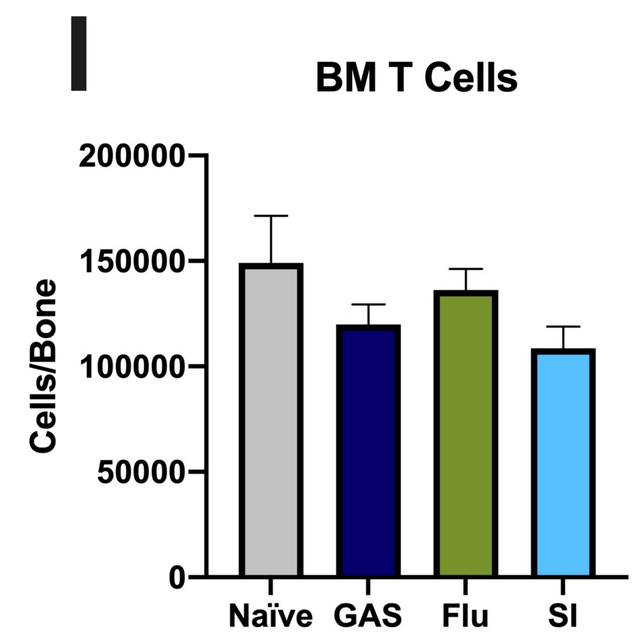

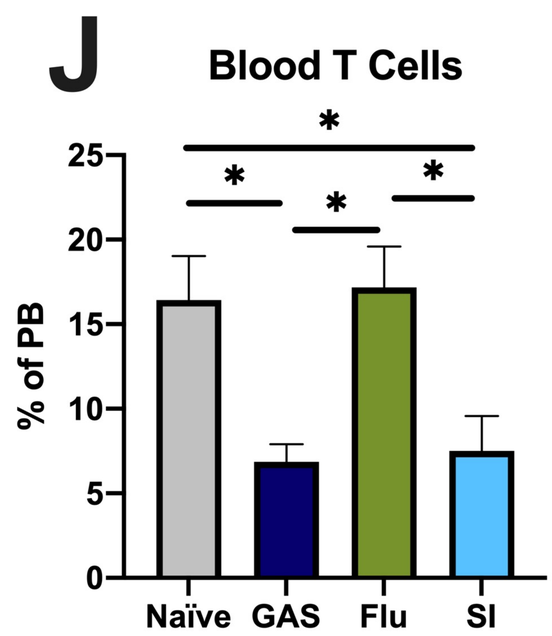

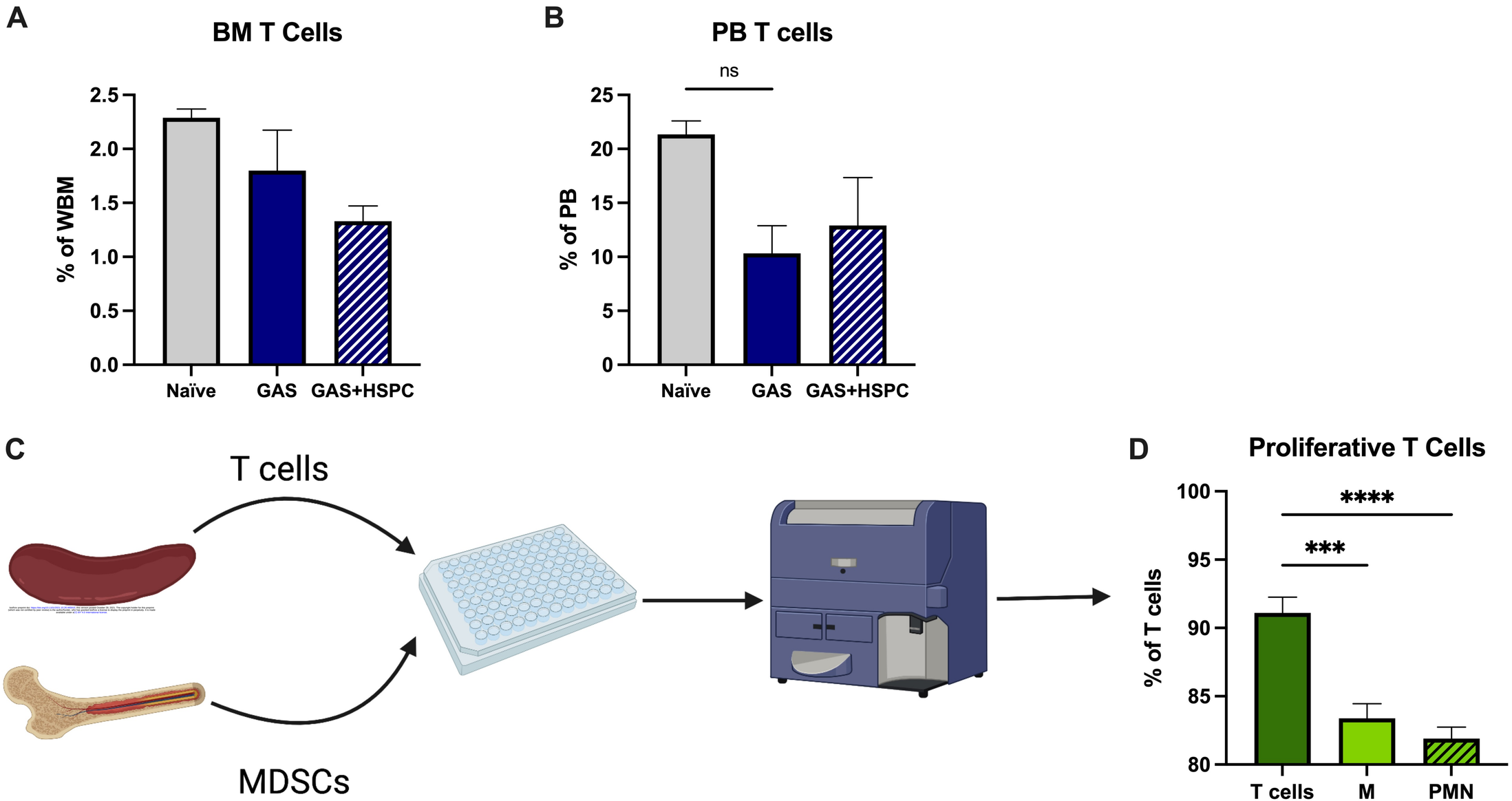
A
BM T Cells
% of WBM
2.5
2.0
1.5
1.0
0.5
0.0
Naïve
GAS
GAS+HSPC
B
PB T cells
ns
% of PB
25
20
15
10
5
0
Naïve
GAS
GAS+HSPC
C
T cells
MDSCs
D
Proliferative T Cells
****
***
% of T cells
100
95
90
85
80
T cells
M
PMN